Estimating Species-Level Aboveground Carbon in Interior Alaska Using Machine Learning and Process-Based Models

by

Wesley E. Rancher

A thesis accepted and approved in partial fulfillment of the

requirements for the degree of

Master of Science

In Geography

Thesis Committee:

Melissa Lucash, Chair

Daniel Gavin, Member

Lucas Silva, Member

University of Oregon

Summer 2025

ABSTRACT

Wesley Rancher

Master of Science in Geography

Title: Estimating Species-Level Aboveground Carbon in Interior Alaska Using Machine Learning and Process-Based Models

Accurate estimates of aboveground carbon in Alaska's boreal forests are essential for tracking ecological change in a rapidly warming region. This study compares two modeling frameworks, 1) an empirically trained Random Forest model driven by remote sensing (RS-RF), and 2) the process-based LANDIS-II model to assess aboveground C trends from 2000 to 2024 across four dominant species: black spruce (*Picea mariana*), white spruce (*Picea glauca*), Alaskan birch (*Betula neoalaskana*), and trembling aspen (*Populus tremuloides*). While both models provided valuable insights, they diverged in their representation of carbon dynamics. RS-RF predicted lower carbon with less temporal variability, whereas LANDIS-II projected higher carbon accumulation and greater temporal variability. The models differed in species dominance rankings and spatial change patterns: RS-RF estimated that trembling aspen had the highest biomass while LANDIS-II estimated white spruce had more biomass than the other species. Variable importance analyses revealed contrasting model sensitivities. RS-RF was shaped by spectral and topographic inputs, especially post-fire indices for birch, whereas LANDIS-II was driven by internal ecological processes like fuel dynamics and biomass pools from dead wood and fine fuels. These discrepancies highlight how each model captures different aspects of forest carbon dynamics. RS-RF excels at detecting observed, near-term responses and localized spatial shifts, while LANDIS-II offers process-based insights into longer-term change and broader landscape trajectories**.** Integrating these approaches can help resolve key uncertainties in boreal carbon modeling and improve our understanding of species-specific trajectories under climate and disturbance pressures.

ACKNOWLEDGMENTS

I would like to express my deepest gratitude to my advisor Dr. Melissa Lucash, for their guidance and support throughout this project. Their mentorship was instrumental in shaping the direction of this research and my growth as a scientist. I am also grateful to the members of my thesis committee, Dr. Dan Gavin, and Dr. Lucas Silva, for their thoughtful feedback, patience, and encouragement.

Special thanks to the Terrestrial Ecosystem Ecology and Ecological Landscapes Lab (TEEL), whose collaborative spirit and technical insight pushed me forward on this project.

I also thank the field crews at Bonanza Creek Experimental Forest and the Cooperative Alaska Forest Inventory (CAFI), for their invaluable work in collecting the data that underpins this research.

To the Department of Geography at the University of Oregon, thank you for providing an inspiring academic home, generous funding support, and a welcoming community. I've learned so much from my fellow graduate students, faculty, and staff who have been both intellectually and personally supportive during my time here.

Finally, I'm grateful to my family and friends for their unwavering support, and to the many people; collaborators, instructors, mentors, and peers who offered time, tools, ideas, or encouragement along the way.

TABLE OF CONTENTS Page

LIST OF TABLES

LIST OF FIGURES

1. INTRODUCTION

Boreal forests encircle the high northern latitudes and represent one of the largest terrestrial biomes on Earth, comprising roughly 25% of global forest cover (Wells et al., 2020). These ecosystems play a critical role in the global carbon cycle, storing about one-third of terrestrial carbon in both biomass and soil organic matter (Apps et al., 1993; Pan et al., 2011). However, the stability of this vast carbon sink is increasingly uncertain as climate warming progresses more rapidly in boreal regions, with warming rates that are two to three times faster than other regions (Chapin et al., 2008; Masson-Delmotte et al., 2021). Given this amplified warming is projected to continue, boreal forests are likely to undergo significant ecological changes, making them a priority for climate change research.

Notably, interior Alaska is an example of a boreal region undergoing rapid ecological change due to rising temperatures and intensified disturbance regimes (Walsh et al., 2017). Wildfire, a dominant force shaping boreal landscapes, is becoming more frequent and severe, disrupting successional trajectories, altering soil conditions, and modifying vegetation structure (Kasischke et al., 2010; Turetsky et al., 2011). These dynamics are contributing to shifts in forest composition, including transitions from historically dominant coniferous species such as black and white spruce to more disturbance-adapted hardwoods like Alaskan birch and trembling aspen (Alexander et al., 2012; Johnstone et al., 2010b). The ecological and carbon consequences of such transitions remain poorly quantified, especially at high latitudes, yet accurately quantifying these shifts is vital for predicting regional carbon budgets and developing effective climate adaptation strategies (Fisher et al., 2014).

Remote sensing has become a key tool for monitoring aboveground carbon (C) and vegetation dynamics across broad spatial and temporal scales. Advances in multispectral imagery, particularly from optical sensors like Landsat, have enabled large-scale assessments of forest structure and biomass over time (Lamping et al., 2025; Lefsky et al., 2002). This empirical, data-driven approach excels at capturing observed landscape conditions and immediate responses to disturbance. Simultaneously, the rise of machine learning (ML) has emerged as a powerful framework for estimating forest attributes using complex predictive algorithms (Breiman et al., 2002; Cutler et al., 2007). The coupling of RS and ML technologies provides a useful framework for generating ecological products rooted in empirical data, at scale (Tian et al., 2023). However, while powerful

for interpolation and mapping current states, RS-ML methods do not capture underlying ecological processes or accurately project future conditions beyond observed ranges.

Process-based models such as LANDIS-II, provide an approach to simulate vegetation dynamics based on ecological mechanisms like succession and disturbance (Scheller et al. 2007; Scheller & Mladenoff, 2004). These models are particularly valuable for exploring long-term ecosystem responses to climate change and management scenarios (Gustafson, 2013). This mechanistic approach allows for a deeper understanding of cause-and-effect relationships and the projection of novel future conditions. Despite their strengths, LANDIS-II and similar models rely on extensive parameterizations and complex calibrations that may lead to large uncertainties (Simons-Legaard et al., 2015). Therefore, while strong in process representation, they often require robust empirical data for initialization and extensive calibrations across a range of processes to ensure realistic outputs (Reese et al., 2025).

In interior Alaska, prior applications of remote sensing and process-based modeling have provided insights into forest recovery and carbon dynamics post-disturbance (e.g. Mekonnen et al., 2019; Shenoy et al., 2011), but no studies have systematically compared these approaches across species to evaluate their respective accuracies, sensitivities to environmental drivers, or implications for detecting ecological change. To improve our understanding of uncertainties in current model estimates of aboveground C and how it has changed in the past two decades across interior Alaska, this study compares aboveground C estimates from a remote sensing–random forest (RS-RF) model and the process-based LANDIS-II model across four dominant boreal species from 2000 to 2024.

The study evaluates four hypotheses: (1) the RS-RF model will provide more accurate estimates of total and species-level aboveground C than LANDIS-II when evaluated against two independent plot datasets, (2) LANDIS-II will project greater variability and 3) larger conifer declines over the 25 year period due to its process-based structure, and (4) RS-RF and LANDIS-II will identify different sets of key drivers for each species, leading to different inferences about the causes of aboveground C dynamics. This study aims to enhance understanding of boreal forest carbon dynamics by comparing two fundamentally different modeling approaches: one data-driven

and empirical, the other process-based, and evaluating their respective strengths and limitations for assessing ecological change in interior Alaska.

2. METHODS

2.1 Study Area

The study region (Figure 1) encompasses 8.7 million hectares, located in interior Alaska, approximately bounded by the Yukon River to the north and the Tanana River to the south. This landscape is topographically complex, ranging in elevation from 3 to 2,196 meters, with an average slope of 10° (Tadono et al., 2014). It features extensive floodplains and braided river systems that intersect rolling hills (Van Cleve et al., 1983). Interior Alaska experiences a continental subarctic climate, with cool, dry winters and hot, dry summers. Temperatures range from -70°F to 35°F (Hinzman & Viereck, 2006). Most precipitation occurs in late summer to early fall with an average annual of 286 mm, 35% of which falls as snow (Hinzman & Viereck, 2006). Wildfire is the dominant natural disturbance, typically occurring as stand-replacing events, with a historical fire return interval (FRI) of 105 to 159 years (Kasischke et al., 2022; Payette, 1992; Viereck, 1973). The region's vegetation is a mosaic of coniferous and deciduous trees, shrubs, and mosses, underlain by discontinuous permafrost (Osterkamp & Romanovsky, 1999; Viereck et al., 1983). The dominant tree species are conifers species like black and white spruce (*Picea mariana & Picea glauca*). Deciduous species such as Alaskan birch (*Betula neoalaskana*) and trembling aspen (*Populus tremuloides*) also occur broadly across the landscape and are often considered an early successional stage of a spruce forest (Van Cleve & Viereck, 1981).

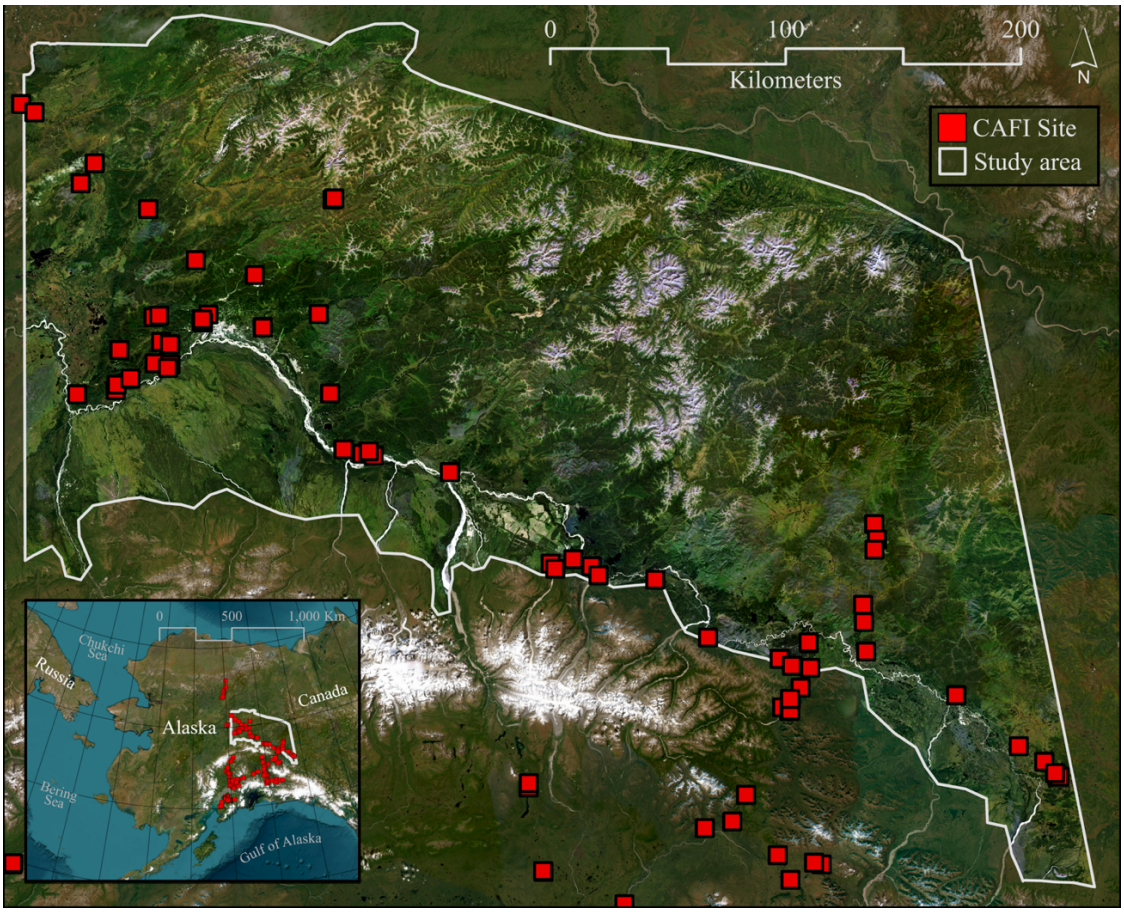

Figure 1: *Study area in interior Alaska, approximately bounded by the Yukon River to the north and the Tanana River to the south. Yellow points indicate field measurement sites with repeated observations from 1994 to 2017 across multiple species.*

2.2 Remote Sensing and Machine Learning

2.2.1 Field Data

Field data, used to train the random forest models, were collected by the Cooperative Alaska Forest Inventory (CAFI) between 1994 and 2017 and are available through the Bonanza Creek LTER database (Van Cleve et al., 2023). Diameter at breast height (DBH) measurements for individual trees were used in species-specific allometric equations to estimate aboveground biomass (Jenkins et al., 2004). Estimates were summed at the plot level; each CAFI plot is 0.04 ha (400 m^2). Four focal species with the most consistent representation across sites and years were selected for analysis: *Betula neoalaskana*, *Picea mariana*, *Picea glauca*, and *Populus tremuloides* (Figure 2).

Separately, forest inventory data collected by the U.S. Forest Service's Forest Inventory and Analysis (FIA) program were used by Weiss et al. (2023) to generate initial conditions in the LANDIS-II simulations (described in Section 2.3.2.2). While both datasets include species-level biomass estimates, they differ in sampling design, spatial extent, and representativeness. These differences should be considered when interpreting comparisons to model outputs.

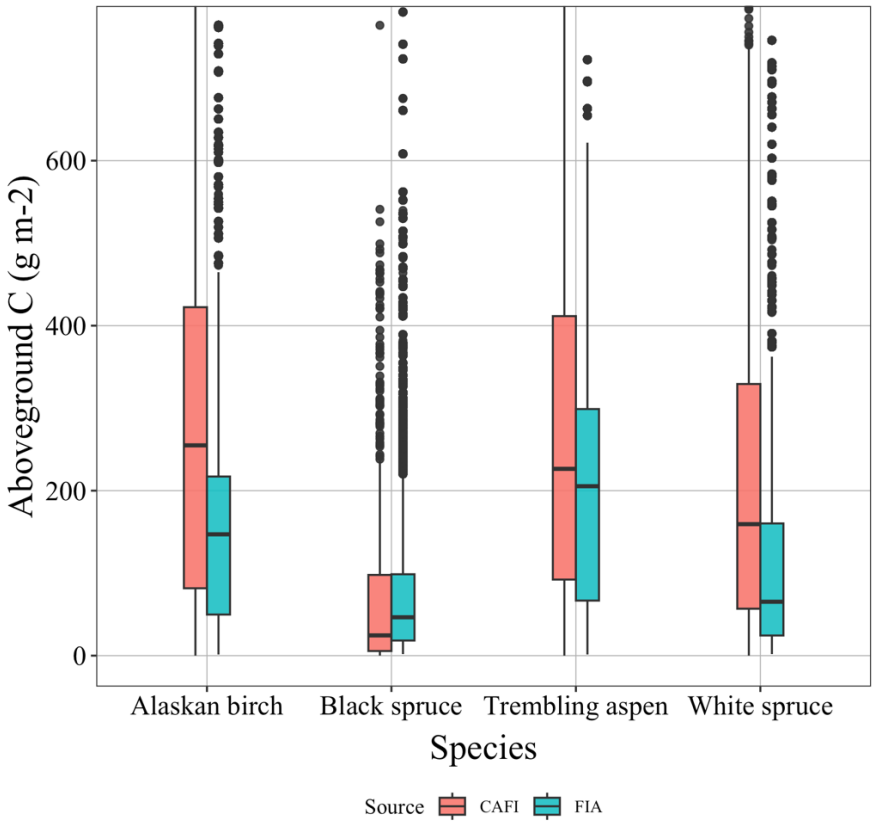

Figure 2. *Distribution of measured aboveground carbon (g C m⁻²) for four dominant boreal tree species: black spruce (Picea mariana), white spruce (Picea glauca), Alaskan birch (Betula neoalaskana), and trembling aspen (Populus tremuloides). Estimates are based on plot-level measurements from the Cooperative Alaska Forest Inventory (CAFI; 0.04 ha plots) and the Forest Inventory and Analysis program (FIA; approximately 1 ha plots). Boxplots show the median, interquartile range (25th to 75th percentiles), and whiskers extend to the nearest observed value within the 5th and 95th percentiles. Points beyond these bounds represent outliers.*

2.2.2 Data Preprocessing

Landsat surface reflectance products were selected due to the satellite's moderate spatial resolution (30-m) with sufficient temporal coverage over the study period (16-day to 8-day return interval) (Wulder et al., 2022), and well-documented use in the literature for classification and regression methods (Boston et al., 2022; Li et al., 2020; Orndahl et al., 2025). Landsat imagery was acquired and preprocessed using Google Earth Engine (GEE, Gorelick et al., 2017). Different image preprocessing algorithms were combined for cloud masking, sun canopy sensor topographic correction (SCSc), and image enhancement (Hurni et al., 2019; Massey et al., 2023; Soenen et al., 2005). Multiband seasonal composite images (Table 1) were generated for spring, summer, and fall of each year from 2000 to 2024, and pixel values were extracted. Each CAFI plot (0.04 ha)

was matched to the corresponding Landsat pixel (30 × 30 m), and a single pixel value was sampled per plot per year. Temporal matching was constrained to the same calendar year in which field measurements were taken, ensuring alignment between remote sensing observations and plot-level aboveground carbon estimates. Spectral indices were calculated for Enhanced Vegetation Index (EVI), Normalized Differenced Vegetation Index (NDVI), Soil Adjusted Vegetation Index (SAVI), Visible Atmospherically Resistant Index (VARI), Modified Normalized Differenced Water Index (MNDWI), and Normalized Burn Ratio (NBR), in addition to tasseled cap brightness, greenness, and wetness. Topography was also accessed in GEE from the JAXA Earth Observation Research Center (Tadono et al., 2014), which is a 30-m resolution product with elevation, slope and aspect. Fire variables were generated from the Monitoring Trends in Burn Severity (MTBS) dataset (citation), where *number of fires* was calculated by counting overlapping burn perimeters in a pixel, and *time since fire* was then determined by extracting the ignition date column of the most recent fire and subtracting it from the sampling year. These fire variables were converted to categorical values (TSF of 0 to 10, 10 to 20, and 20+ years), after finding low importance scores in initial model runs.

2.2.3 Random Forest

The sampled data for model training consisted of aboveground C estimates derived from field measurements (as described in Section 2.2.1 Field Data) spatially joined with corresponding remote sensing, topographic, and fire predictor variables. Specifically, for each field plot with aboveground C measurements, pixel values for the 24 explanatory variables (as summarized in Table 1 and Supplemental 1) were extracted from the annual multiband Landsat composites, topographic layers, and fire history data for the exact location and year of the field observation (1994-2017). This process ensured that each training data point represented a direct empirical link between observed forest carbon and its contemporaneous environmental and spectral characteristics.

Species aboveground C was modeled using multivariate models using all 24 remote-sensing variables. Initial models were assessed using randomForest (Breiman et al., 2002) and K-nearest neighbors, and randomForest was selected as the final model for this study as it yielded the lowest Root-Mean-Squared-Error (RMSE). Machine learning code was written in R using the tidymodels package (Kuhn & Silge, 2022). This package was chosen as it can flexibility fit and predict for a range of models, requiring a formula (target ~ independent variables), model engine (e.g., randomForest, ranger), and mode (classification, regression).

The full dataset of these spatially and temporally matched observations (spanning 1994-2017; some years had missing observations or no records at certain locations) was then combined into one comprehensive dataset and split by species for individual model training. The resulting dataset included 24 explanatory variables (Supplemental 1), with aboveground C (g C m^2) serving as the target variable for the regression models.

Model evaluation involved grid search parameterization (Torre-Tojal et al., 2022), and cross validation (Kuhn & Silge, 2022). Correlated variables were removed using a Pearson coefficient of 0.80 (Benesty et al., 2009; Chen et al., 2024). Grid search was introduced using an expanded grid which applies sequences of values by n increments for tuning the number of variables tried at each split (mtry), the number of trees (ntree), and the minimum number of data points required for splitting (min n). The v-fold cross validation method was used to resample the dataset and find optimal model tuning parameters for each species. Variable importance was

identified using a Gini coefficient (Breiman et al., 2002), where importance is a measure of percent increase in node impurity when removing the variable.

The trained random forest models were then used to generate annual predictions of aboveground carbon (C) across the study area for the years 2000–2024. Predictor variables used in the modeling process derived from Landsat composites, topographic layers, fire history, and climate data were assembled into annual multiband raster stacks corresponding to this period. The final models were evaluated using average RMSE and R^2 across five cross-validation folds and assessed for variable importance (Supplemental Table 1).

Table 1. *Predictor variables used in the remote sensing–random forest (RS-RF) modeling framework prior to collinearity screening and variable selection. Topographic products are treated as static maps so these sources are sampled once during model training and are used at each time step in the prediction process. Spectral indices were derived from Landsat and were atmospherically and topographically corrected.*

Type	Composite Strategy	Variables	Training Image Dates	Source
Topographic	Static	Aspect Elevation (m) Slope	Static	ALOS-1 (30 m)
Fire		TSF 0-10 years TSF 10-20 years TSF 20-25 years	1994-2017	MTBS (30 m)
Spectral	Seasonal (spring, summer, fall)	NDVI EVI TCB, TCG, TCW NBR SAVI VARI MNDWI	1994-2017	Landsat 5-9 (30 m)

2.3 LANDIS-II

2.3.1 Model Overview

Originally developed for simulating forest landscape succession and disturbance (Mladenoff, 2004), LANDIS-II is a spatially interactive and process-based forest landscape model. It provides a modular framework of coupling open-source extensions to model ecosystem processes (Scheller et al., 2007). The model simulates the cooccurrence of ecological processes (i.e., growth, competition, disturbance, mortality, and regeneration), and it has been adopted for use in climate change research in high latitude ecosystems like Alaska and Siberia (Gustafson et

al., 2024; Lucash et al., 2023; Weiss et al., 2023), as well as in the lower 48 and Canada (Nenzén et al., 2020; Sturtevant et al., 2009).

2.3.1.1 DGS

DAMM-MCNiP-GIPL-SHAW (DGS), a coupled model framework designed to simulate vegetation succession, soil hydrology, and permafrost dynamics in boreal ecosystems, was used in this study (Lucash et al., 2023). DGS integrates three core components: 1) DAMM-MCNiP (Dual Arrenius Michaelis Menton and Microbial Carbon and Nitrogen Physiology Model; Davidson et al., 2014, 2012, Finzi et al., 2015, Abramoff et al., 2017), 2) GIPL2 (Geophysical Institute Permafrost Laboratory, Nicolsky et al., 2009; Marchenko et al., 2008), and 3) SHAW (Simultaneous Heat and Water, Flerchinger & Saxton 1989). In DGS, landscape initial conditions are represented as species-age cohorts with associated leaf and wood biomass assigned to each raster cell. DGS calculates monthly growth within each raster cell using species-specific life history attributes (e.g., longevity, moisture response, and leaf area index). The succession algorithms in DGS were built from the Net Ecosystem Carbon and Nitrogen (NECN) model (Scheller et al., 2011), but differ in how they compute water availability and soil temperature. Carbon and nitrogen cycling in NECN follows the CENTURY model where soil C pools were theoretically represented as active, passive, and slow (Parton et al., 1994). DAMM-MCNIP simulates seven measurable C pools with fluxes based on physiological principles (Abramoff et al., 2017). Soil temperature in NECN is calculated using a four-parameter species-specific curve, whereas in DGS, soil temperature is inherited from GIPL (Lucash et al., 2023).

SHAW simulates the vertical transfer of heat, water, and solutes down to 3 m at 75 user-defined depths and is driven by vegetation and snowpack (Flerchinger et al., 2015; Flerchinger & Cooley, 2000; Marshall et al., 2021). It represents hydrologic processes such as ablation, evapotranspiration, infiltration, snow accumulation, and surface runoff (Flerchinger et al., 1994; Flerchinger & Saxton, 1989). These processes are represented with a one-dimensional soil-vegetation-atmosphere column, allowing SHAW to track energy and moisture exchanges from the canopy and snowpack through the soil profile. The model uses a full surface energy balance to simulate snowpack dynamics, applies the Richards equation to estimate water movement through unsaturated soils (Richardson, 1922), and accounts for vegetation-driven transpiration and canopy

interception (Armatas et al., 2018; Jarvis, 1997; Stewart, 1988). Evapotranspiration is estimated using a gradient diffusion approach through a multilayer canopy, with stomatal resistance regulated by Jarvis–Stewart-type controls that respond to environmental factors such as solar radiation, humidity, temperature, and soil moisture (Flerchinger et al., 2015; Stewart, 1988)

GIPL is forced by air temperature and simulates ground temperature, active layer thickness, and talik thickness (Jafarov et al., 2012; Lucash et al., 2023; Weiss et al., 2023). The GIPL numerical model solves a nonlinear heat flow equation that incorporates phase change dynamics (Jafarov et al., 2012) and can simulate subsurface thermal regimes to depths of up to 65 m (Lucash et al., 2023; Weiss et al., 2023). In DGS, soil properties such as thermal conductivity and heat capacity and soil environmental conditions like ice content inherited from SHAW (Lucash et al., 2023).

2.3.1.2 Climate-Social Fire

Climate-Social-Fire was used in this study to simulate the effects of wildfire (Scheller et al., 2019). Social-Climate-Fire relies on four algorithms (i.e., ignitions, spread, intensity, mortality). Ignitions on the landscape follow a supply and allocation model where the supply is generated from a Poisson model (see Section 2.3.2.3), and ignitions are allocated using an ignition surface. Fire spread was simulated using a cell-to-cell probability model based on a logistic function of daily fire spread, which incorporates the Fire Weather Index (FWI), effective wind speed, and fine fuel availability (Scheller et al., 2019).

2.3.1.3 Output Extensions

Two output extensions from LANDIS-II were used to generate biomass output. The Community Biomass Output extension was used in this study for calibrating growth (LANDIS-II Biomass Community Output v3.0 User Guide 2024). This extension produces new initial conditions at specified time steps and was compared against starting conditions to ensure species growth did not diverge substantially from initial conditions at time 0 (Supplemental 2). The Biomass Output extension was used to generate maps of aboveground biomass at a species level (Scheller & Mladenoff, 2004).

2.3.2 Parameterization

2.3.2.1 Climate Data

Daily climate data of air temperature, downward shortwave radiation, precipitation, relative humidity, and wind speed from one GCM (NCAR-CCSM4), were used in this analysis. Climate data for this analysis were sourced from the NCAR-CCSM4 global climate model, dynamically downscaled to 20 km resolution using the Weather Research and Forecasting (WRF) model by the Scenarios Network for Alaska and Arctic Planning (SNAP) (Bieniek et al., 2016; Lader et al., 2017). The climate data used in this analysis represents a historical scenario (no climate change/ little climate change). The historical scenario was simulated in LANDIS-II for the period 2000–2024 by using sequenced daily climate data from the 1970–1999 baseline period to reflect a stationary climate (i.e., no or minimal climate change).

Although the downscaled data incorporate elevation and spatial climate variability, LANDIS-II requires climate inputs to be organized by climate regions rather than gridded cells (Scheller et al., 2007). In this study, 10 climate regions were defined across the landscape, with each region assigned a time series from the most representative 20 km WRF grid cell. This approach maintained broad spatial patterns in the climate data while conforming to the region-based requirements of the model.

2.3.2.2 DGS Calibration

An initial biomass map was created by imputing species cohorts with biomass density and age (Weiss et al. 2023) from Forest Inventory and Analysis (FIA) data (Cahoon et al., 2022) using vegetation and wetland landcover classification data (Alaska Center for Conservation Science 2017). The most recent version of LANDIS-II (v8) requires inputs of both woody and leaf biomass. Average foliar ratios for each species were calculated from Forest Inventory and Analysis (FIA) data using DBH measurements and Jenkins coefficients (Jenkins et al., 2004). These ratios were then multiplied by initial cohort biomass to obtain leaf and wood biomass for the starting conditions of the model. In LANDIS v8, light establishment parameters replace shade tolerance classes used in v7 and are species-specific instead of at a functional level (v7). This required fitting seedling data from FIA to a Weibull distribution (Fleming, 2001), and obtaining the scale and shape parameters of each species' curve (Supplemental S3). This step ensured that species

establishment was responsive to light availability, a critical factor influencing regeneration dynamics and competitive interactions in boreal forests.

2.3.2.3 Climate-Social Fire Calibration

To calibrate ignitions, probability of ignitions coefficients were calibrated to empirical data by Weiss et al., 2023a. This involved fitting the simulated fire weather index (FWI) from LANDIS-II to lightning occurrences in the region from a spatial fire occurrences database (Short, 2014) using a Poisson model (Supplemental S4). Maximum daily spread area was calculated using a generalized linear model relating historical daily fire area to FWI and wind speed. These parameters were originally fit by Weiss et al 2023, using historical fire perimeter data (GeoMAC 2019, 2020), meteorological station data (Menne et al. 2012), topography (USGS 2020a), and fine fuels data (USGS 2020b), with minor adjustments to the ignition and spread intercepts to match historical fire records for the landscape.

2.4 Analysis

Annual aboveground C estimates were produced from both RS-RF models and LANDIS-II simulations between 2000-2024 to compare carbon dynamics between CAFI data and each modeling approach. This dual modeling framework supports evaluation of total and species-level carbon trends (H1), differences in variability of over time (H2) changes in relative dominance (H3), and the contrasting role of disturbance (particularly wildfire) in driving aboveground C (H4). Values reported are means with standard deviation.

2.4.1 Remote sensing and LANDIS-II Carbon Estimates

RS-RF models generated annual species-level carbon estimates from 2000-2024 using spectral, topographic, and climate predictors. Due to computational constraints, predictions were made on a spatially stratified subset (~1%) of each annual image (Supplemental 5). This subset was designed to capture landscape heterogeneity and temporal change efficiently. Spatially complete maps were also produced for 2002 and 2022 to support spatial comparisons.

LANDIS-II v8 simulations were run in a Linux container on a high-performance computing cluster (Hancock et al., 2021). Maps generated from the Biomass Output extension

(Section 2.3.1.3) were converted to units of carbon (g C m^{-2}) and sampled systematically using the same spatial schema applied to the remote sensing estimates. Annual values from 2000–2024 were averaged across 3 replicates for each species then compared directly to RS-RF derived carbon estimates.

2.4.2 Comparing Model Structure and Driver Importance

To assess differences in model structure and the influence of drivers (H3), a second set of RF models was trained on LANDIS-II output at CAFI plot locations. Predictor variables included initial maps (e.g., topographic, hydrology), climate, and outputs from disturbance-related extensions (DGS, Climate-Social-Fire). Models followed the same fitting framework used in the RS-RF pipeline (Section 2.2.3), allowing for controlled structural comparison.

3. RESULTS

For brevity, RS-RF model accuracy metrics are reported in Supplemental Table 1. Overall, model performance was strongest for black spruce (R^2 = 0.75) and weakest for trembling aspen (R^2 = 0.42, Supplemental Table 1).

3.1 Total and Species-Level Aboveground C

Year 2000 marked the beginning of the simulation, and biomass values from the CAFI and FIA datasets were summarized across their respective vegetation plots, which differ in sampling design. These values were compared to the LANDIS-II output, which represents FIA-derived biomass imputed across the CAFI plot network (Figure 3). CAFI plots had a mean aboveground C of 188.76 g C m^{-2} (SD = 211.6 g C m^{-2}). The FIA dataset reported a 63% higher total (mean: 307.7 g C m^{-2}, SD= 468.32 g C m^{-2}) relative to CAFI. RS-RF predicted a mean of 215.33 g C m^{-2} (SD= 140.8 g C m^{-2}) which was 14% higher than CAFI and 30% lower than FIA. The LANDIS-II model projected the highest total aboveground C between the models, with a mean of 478.25 g C m^{-2} (SD = 832.7 g C m^{-2}), a value 153% and 55% higher than CAFI and FIA, respectively.

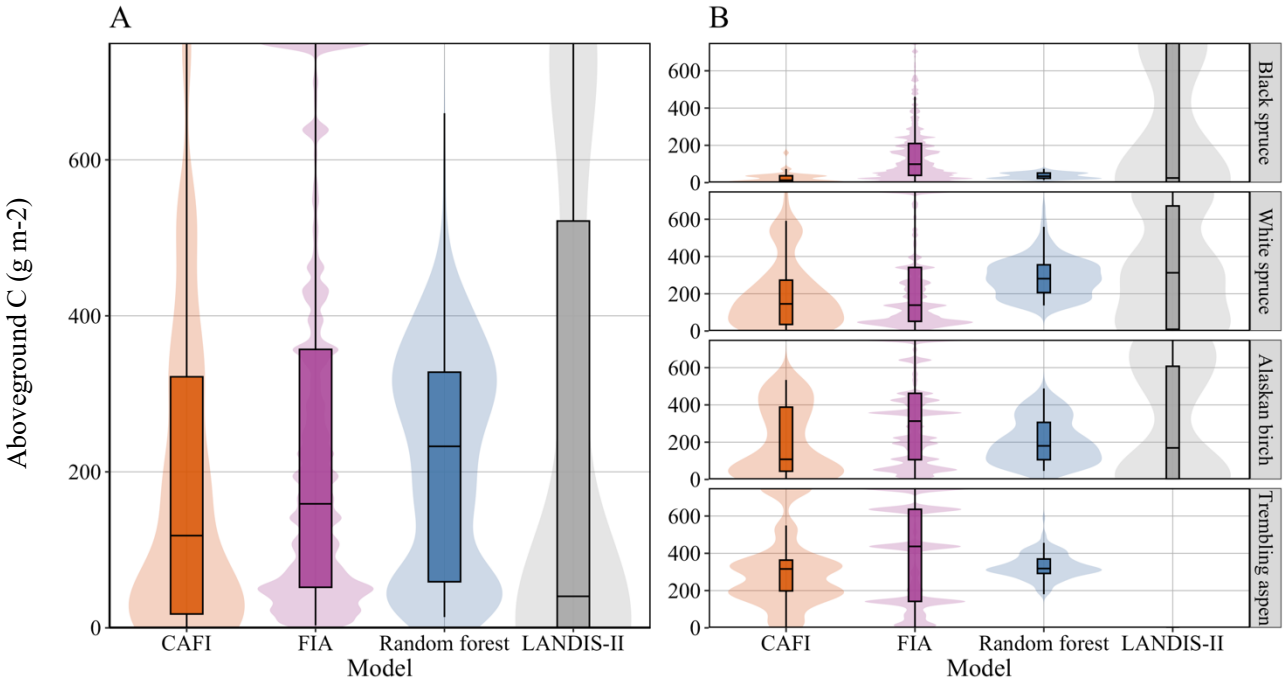

Figure 3. *Empirical and simulated aboveground carbon in year 2000. Panel A shows total carbon across all species, and Panel B disaggregates the distributions to a species level. Empirical data are shown in orange (CAFI: used to train RS-RF models) and pink (FIA: used for initial conditions in LANDIS-II), each summarized across their respective field plots, which differ in sampling design. Simulated data across the CAFI plot network are shown in blue for RS-RF and gray for LANDIS-II. LANDIS-II estimates represent FIA-derived values imputed across the full landscape, which may alter the distribution relative to plot-level summaries. Some outliers omitted as they did not fit within the plot range.*

Across the full time series from 2000 to 2017 (Figure 3A), aboveground C from CAFI observations (orange bars) averaged 646.7 ± 155.8 g C m^{-2}, while average RS-RF estimates (Figure 3A, blue bars) were 23% higher at 801.45 ± 118.22 g C m^{-2}. LANDIS-II projected a 105% higher mean with more variability (1,320.22 ± 274.43 g C m^{-2}). These differences are also reflected in the species-level carbon distributions in Figure 4B and outlined below.

For conifer species across the study period, black spruce observed aboveground C from CAFI averaged 52.39 ± 50.56 g C m^{-2}. RS-RF predicted a 24% lower mean C estimate of 39.63 ± 20.47 g C m^{-2}. While LANDIS-II projections were 567% higher than CAFI and more variable, with a

mean of 349.45 ± 442 g C m^{-2}. These patterns were reflected in model performance statistics (Table 2), where RS-RF showed negligible correlation with CAFI observations (R^2 = 0.02) but lower RMSE (65.1) than LANDIS-II (R^2 = 0.19; RMSE = 59.2). The observed mean for white spruce was 274.23 ± 185.1 g C m^{-2} (Figure 3B). RS-RF produced an 11% higher mean of 304.46 ± 133.1 g C m^{-2}, compared to CAFI. LANDIS-II projections were 101% higher than CAFI and more variable at 551.7 ± 718.1 g C m^{-2}. RS-RF exhibited stronger correspondence with CAFI observations (R^2 = 0.21) than LANDIS-II (R^2 = 0.13; Table 2).

For hardwood species**,** Alaskan birch CAFI observed aboveground C was an average of 173.52 ± 149.35 g C m^{-2} (Figure 3B). Estimates from RS-RF averaged 198.54 ± 127.11 g C m^{-2}, a value 14% higher than the CAFI data. LANDIS-II projected a 168% higher and more variable mean of 464.64 ± 622.71 g C m^{-2}. RS-RF estimates were more closely aligned with CAFI observed values (R^2 = 0.21 vs. 0.11 for LANDIS-II; Table 2). For trembling aspen, observed aboveground C averaged 219.33 ± 112.44 g C m^{-2} (Figure 3B). RS-RF estimates were 33% higher at 292 ± 72.54 g C m^{-2}. In contrast, LANDIS-II projected a 96% lower mean of 9.33 ± 21.37 g C m^{-2}. RS-RF demonstrated the strongest relationship to empirical observations compared to other species (R^2 = 0.33, p = 0.045).

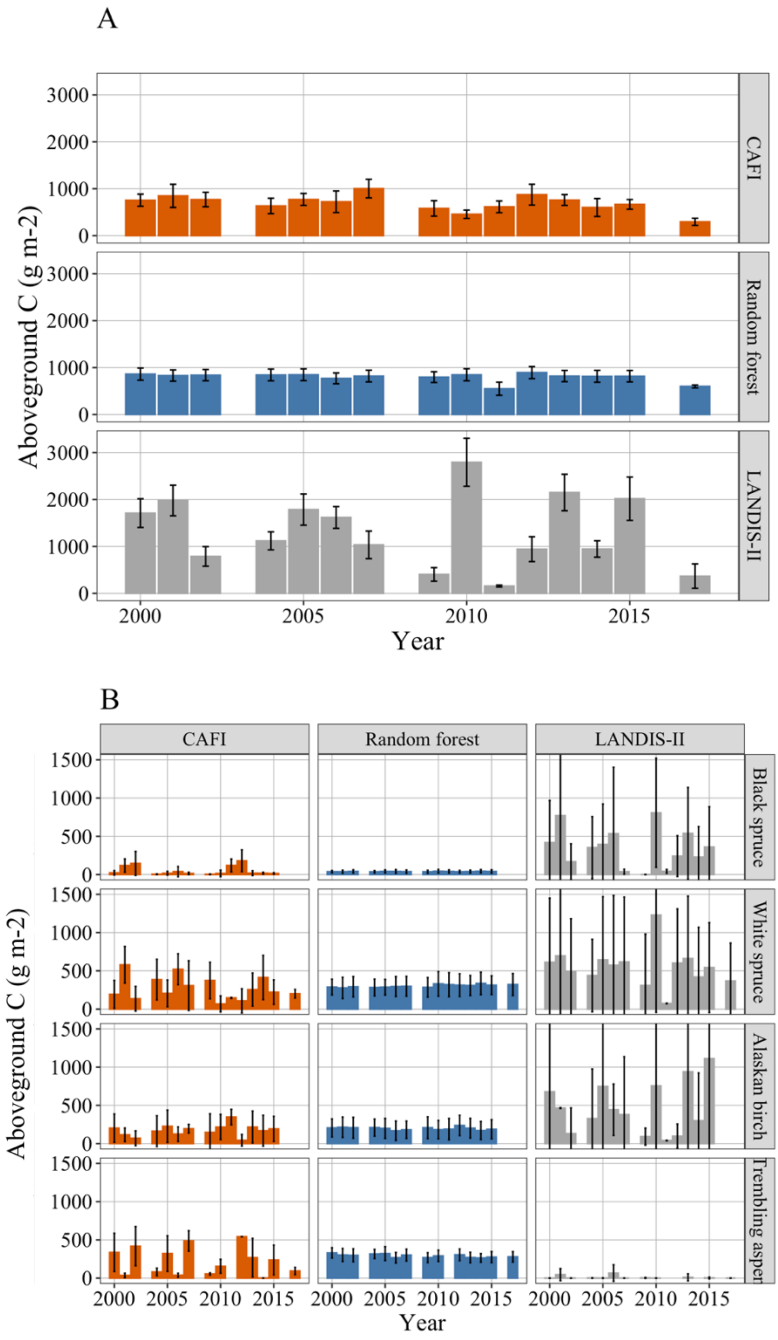

Figure 4. *Time series of A) total landscape carbon (g C m^{-2}) and B) landscape total aboveground C at a species level between models. Estimates are from the RS-RF model (blue bars and lines) and the LANDIS-II model (gray bars and lines) and observed measurements (orange bars and lines) at resampled permanent CAFI plots. Years with missing data indicate years for which no field measurements were available (varies by species). Data shown spans 2000-2017.*

***Table 2**. Species-specific model performance comparing carbon estimates from LANDIS-II and the RS-RF model against observed CAFI values. Metrics reported include the coefficient of determination (R^2), root mean square error (RMSE), and p-value for the model-predicted carbon. Higher R^2 and lower RMSE indicate better agreement with observations. Statistically significant relationships ($p < 0.05$) are highlighted for Trembling aspen using the RS-RF model.*

Species	Model	R^2	RMSE	P-value
Black spruce	Random forest	0.02	65.1	0.855
	LANDIS-II	0.19	59.2	0.156
White spruce	Random forest	0.21	146.0	0.176
	LANDIS-II	0.13	152.0	0.376
Alaskan birch	Random forest	0.21	72.1	0.165
	LANDIS-II	0.11	77.0	0.451
Trembling aspen	Random forest	0.33	160.0	0.045
	LANDIS-II	0.08	188.0	0.390

3.2 Changes in Relative Species Dominance

Change in aboveground carbon for black spruce (Figure 5A, top panel) indicated minimal, albeit increasing, trends over the study period with the RS-RF model. An estimated 40% of the model landscape gained between 1-10 g C m^{-2}, while 25% of the landscape lost between 1-10 g C m^{-2}. Losses were concentrated in the central and southern regions. In contrast, LANDIS-II changes for black spruce (Figure 5B, top panel) showed a greater magnitude of change. Twenty-three percent of the landscape experienced losses greater than 100 g C m^{-2}, and 23% of the landscape experienced gains greater than 100 g C m^{-2}. Thirty-two percent of the landscape however, changed very little (-1 to 1 g C m^{-2}). Regions that gained C in LANDIS-II generally corresponded to areas that gained using the RS-RF approach.

White spruce change estimated from RS-RF (Figure 5A, second panel) showed that 23% of the landscape gained between 10-50 g C m^{-2}, while 21% of the landscape lost C in that same range. An additional 20.5% of the landscape experienced losses greater than 50 g C m^{-2}. Losses were concentrated central and northwestern areas, while gains were more spatially dispersed with some clustering in the south. LANDIS-II (Figure 5B, second panel) projected higher gains. 26.5% of the landscape gained C greater than 100 g C m^{-2}, while 12.5% lost greater than 100 g C m^{-2}. Most of the landscape (40%) showed minimal change (-1 to 1 g C m^{-2}). Losses were concentrated in the central to western regions, while gains were dispersed, slightly favoring the east.

RS-RF change estimates for Alaskan birch (Figure 5A, third panel), revealed that 44% of the landscape gained between 10–100 g C m^{-2}, and 12% gained greater than 100 g C m^{-2}. Only 10% of the landscape lost more than 10 g C m^{-2}, and 28% remained stable (−1 to 1 g C m^{-2}). Gains were concentrated in central and southwest regions. LANDIS-II (Figure 5B, third panel) also showed extensive increases: 39% of the landscape gained 10–100 g C m^{-2}, and 19% gained greater than 100 g C m^{-2}. Just 6% of the landscape lost more than 10 g C m^{-2}. Alaskan birch gains were more uniformly distributed in LANDIS-II, with some clustering along the Tanana River (dense black cells).

Trembling aspen depicted decreases in certain hotspots on the landscape for the RS-RF model (Figure 5A, bottom panel) and little to no change in LANDIS-II (Figure 5B, bottom panel). RS-RF predicted 25% of the landscape had gained greater than 1 g C m^2, while 45% of landscape lost between 10 and 50 g C m^{-2}. Increases occurred in the northwest and decreases occurred in the southern and eastern regions. LANDIS-II in contrast, projected less variability and an increasing trend. 89% of the landscape lost between −1 to 1 g C m^{-2}, while only 2% and 1% showed gains and losses greater than 10 g C m^{-2}, respectively. Nine percent of the landscape experienced gains greater than 100 g C m^2.

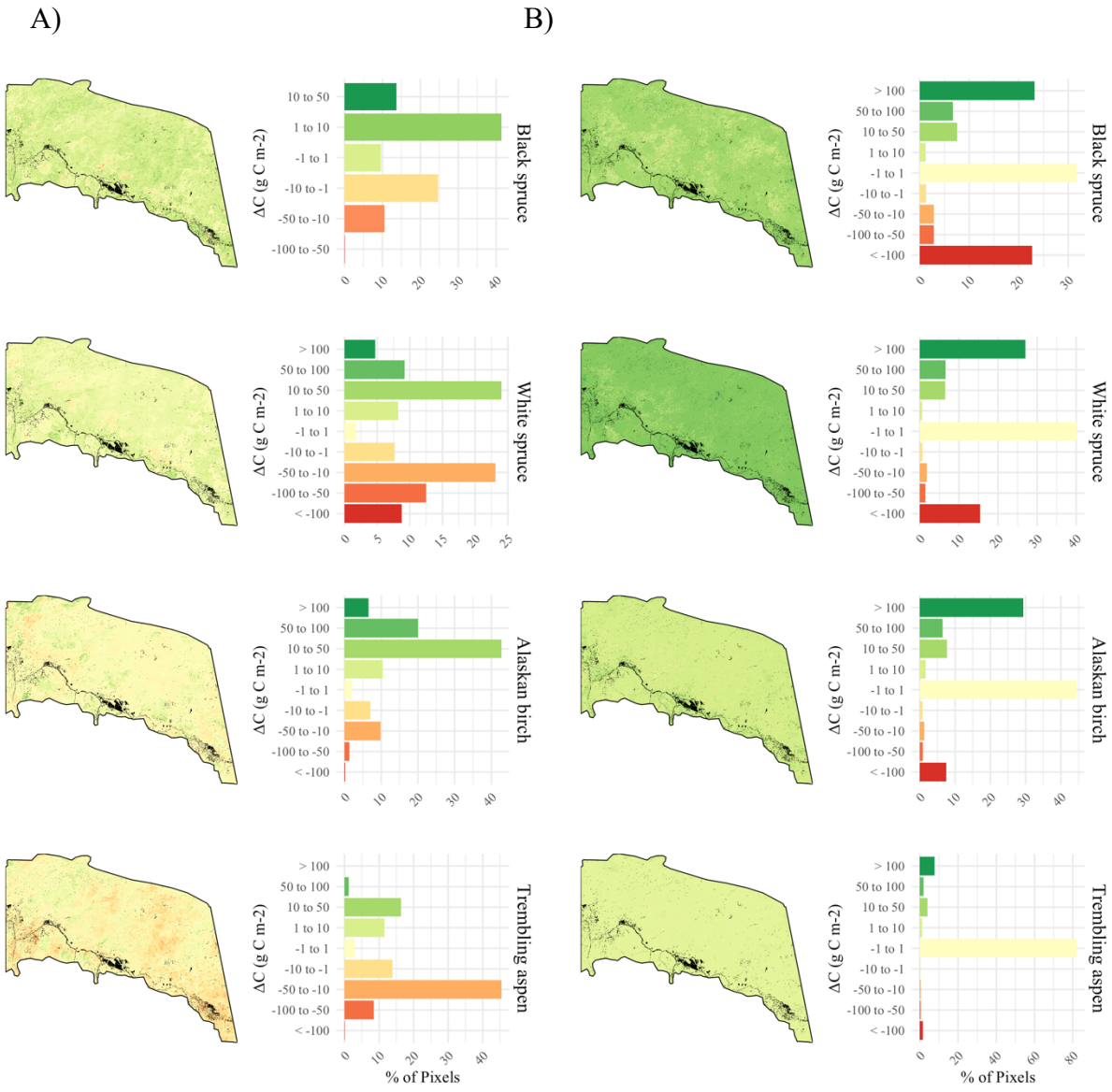

Figure 5. *Species-specific changes in aboveground carbon (Δ aboveground C; g C m^{-2}) from 2000–2004 to 2020–2024 modeled by (A) RS-RF and (B) LANDIS-II. Each row represents a different species (black spruce, white spruce, Alaskan birch, trembling aspen). Left panels show spatial distributions of Δ aboveground C, while right panels show the percentage of pixels falling into Δ aboveground C bins. Green bars indicate increases in aboveground C, red bars indicate declines, and yellow bars show minimal change.*

Percent area of the landscape where conifer species (black spruce and white spruce) declined and where hardwood species (Alaskan birch and trembling aspen) increased within each model was evaluated. RS-RF predicted widespread conifer decline (91.5%) and hardwood expansion (94.4%), while LANDIS-II projected more moderate changes, with 60.8% of pixels showing conifer loss and 58.8% showing hardwood gain.

Table 3. *Percent of landscape where conifer species declined and hardwood species increased, based on RS-RF and LANDIS-II estimates. "Conifer Loss" includes pixels where black spruce or white spruce showed net decline; "Hardwood Gain" includes pixels where Alaskan birch or trembling aspen showed a net increase.*

% of Pixels	**RS-RF**	**LANDIS-II**
Conifer Loss	91.5%	60.8%
Hardwood Gain	94.4%	58.8%

3.3 Model Drivers of Aboveground C

Variable importance was measured for the RS-RF model (Figure 6, Panel A). Spatial and topographic variables (e.g., latitude, longitude, digital surface model) were most important for black spruce. For white spruce, summer spectral indices such as tasseled cap brightness (tcb_summer), wetness (tcw_summer), and enhanced vegetation index (evi_summer) were most influential. Alaskan birch was most strongly associated with post-fire spectral indices, especially summer normalized burn ratio (nbr_summer). Trembling aspen showed greater importance of spatial and topographic variables (e.g., latitude, longitude, digital surface model).

When variable importance was measured from an additional RF model built using LANDIS-II outputs, the results were broadly consistent across species (Figure 6, Panel B). Deadwood was the most influential predictor for all species, while other variables played secondary roles. For Alaskan birch, however, deadroots emerged as a notably important driver alongside deadwood and fine fuels. Black spruce was also influenced by aspect, while white spruce estimates were linked to carbon sequestration rates (net ecosystem exchange, NEE) and leaf area index (LAI). Trembling aspen showed greater sensitivity to growing season length (GSL) and prevailing wind direction (northing/easting).

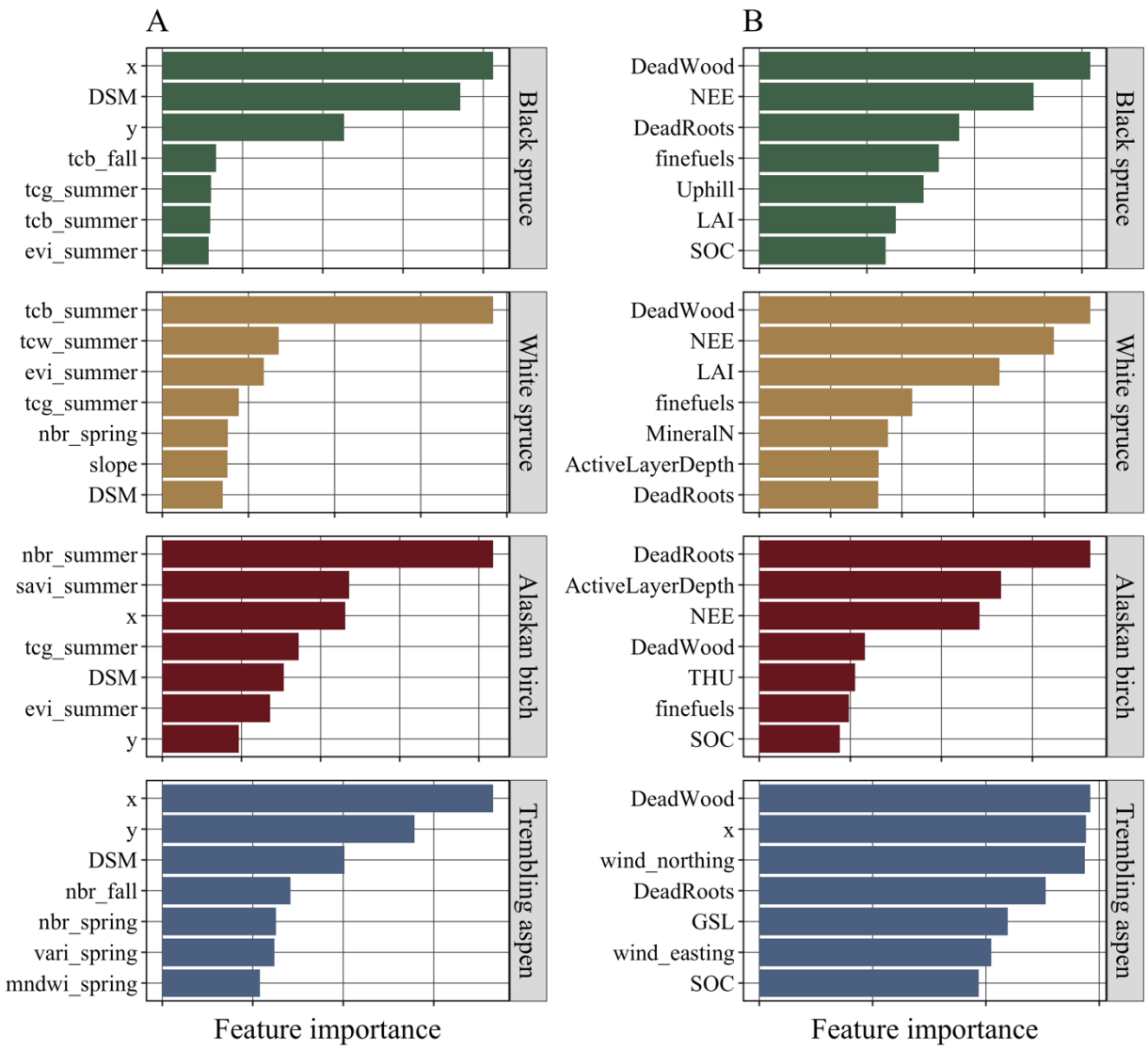

Figure 6. *Relative importance of environmental and spectral predictor variables in the RS-RF (panel A) and ecological features in the LANDIS-II (panel B) models for predicting aboveground C across four dominant boreal tree species: Alaskan birch, black spruce, trembling aspen, and white spruce. Variable importance in both models is based on the mean decrease in Gini impurity.*

4. DISCUSSION

4.1 Comparing Model Estimates to Observations

Differences in the behavior and design of the RS-RF and LANDIS-II models shaped the spatial and temporal patterns of predicted aboveground carbon across the study landscape. As expected, the remote sensing–random forest (RS-RF) approach produced estimates with low temporal variability, while LANDIS-II simulated more variable carbon trajectories over time. This

pattern reflects the models' contrasting structures: RS-RF is empirical and data-driven, capturing annual variability detectable in spectral data, whereas LANDIS-II is a process-based simulation that models long-term carbon accumulation from mechanistic assumptions.

Hypothesis 1, which proposed that the RS-RF model would provide aboveground C estimates which were more similar to CAFI plots than LANDIS-II, was supported. RS-RF estimates of total aboveground carbon generally aligned more closely with observed CAFI data, a finding that is expected given the RS-RF model's empirical nature and its training directly on a subset of the CAFI field observations used for comparison. Moreover, in the baseline year 2000, RS-RF estimates were closer to FIA estimates (Figure 3), which was the empirical source used for generating initial conditions within LANDIS-II. This aligns with previous research highlighting the strengths of empirical, remote sensing-based models in capturing observed conditions through statistical calibration to field data (Goetz et al., 2009). Specifically, Goetz et al. describe how direct remote sensing approaches, which apply machine learning algorithms like regression trees to satellite observations, can produce spatially continuous, pixel-level estimates of AGB with high fidelity to field data, especially in landscapes with fine-scale heterogeneity or disturbance.

Conversely, LANDIS-II consistently projected lower carbon than both CAFI and FIA plots, which is inconsistent with the second part of H1. Estimates from LANDIS were greater than the RS-RF model and displayed greater interannual variability, consistent with H2 (Figure 4). These differences reflect the contrasting assumptions and input dependencies of each model. While RS-RF leverages spectral data to produce annual, static predictions, LANDIS-II simulates vegetation and carbon dynamics mechanistically over time, based on initial conditions from FIA data and thematic landcover maps. This distinction mirrors the challenges Goetz et al. highlight with the "combine and assign" approach, which, while spatially explicit, is sensitive to the quality and representativeness of input data layers and may overgeneralize AGB within landcover types.

4.2 Assessing Species-Level Carbon

At the onset of the study (2000), the two models yielded completely different rankings of landscape-scale species dominance based on aboveground C. RS-RF indicated trembling aspen as the most dominant, followed by white spruce, and Alaskan birch, and black spruce. LANDIS-II

ranked white spruce as most dominant, followed by Alaskan birch and trembling aspen and black spruce (Figure 4). These discrepancies likely arise from fundamental differences in the methods and data used for model initialization. RS-RF incorporates empirical data directly from CAFI plots alongside satellite-derived spectral and topographic variables, capturing current landscape conditions. In contrast, LANDIS-II is initialized using FIA plots, forest type maps, and landcover classifications, which define initial species distributions but do not explicitly drive local site conditions or fine-scale environmental variation during simulations.

Notably, RS-RF depicted more distinct declines in conifer species across the study period. These declines were most evident in lower elevation and more fire-affected areas, where spectral indicators suggested recent disturbance. In contrast, LANDIS-II projected less pronounced conifer declines. This discrepancy likely reflects differences in model resolution, structure, and initialization. RS-RF's fine-scale (30 m) resolution, combined with its direct use of spectral and topographic variables, may better capture small-scale conifer loss due to disturbance or site-specific stressors. LANDIS-II's coarser 200 m resolution and its reliance on initial forest type maps and broad disturbance parameters may obscure localized declines, particularly in early-successional transitions. Although both models indicate some degree of conifer loss, RS-RF more clearly detects shifts away from spruce dominance. These patterns align with recent observations from Walker et al. (2023) and Weiss et al. (in prep), which document increased vulnerability of spruce in frequently burned stands, supporting the notion that conifer declines are a prominent feature of contemporary boreal change.

Similar to previous studies (Alexander et al., 2012; Johnstone et al., 2010b), widespread losses in coniferous species carbon were observed with both models across the landscape (Table 3), though with greater declines predicted in the RS-RF model than LANDIS-II. Declines in conifer biomass are concerning because they represent a significant loss of long-lived carbon sinks and can alter ecosystem services such as permafrost stability and habitat structure (Johnstone et al., 2010a; Schuur et al., 2015).

4.3 Drivers of Aboveground Carbon

Hypothesis 3 was supported, as RS-RF and LANDIS-II identified distinct drivers of aboveground C across species. Black spruce carbon in the RS-RF model was associated with spatial and topographic variables (latitude, longitude, and DSM), reflecting its relationship with landscape position and location (Johnstone & Kasischke, 2005). White spruce showed strong associations with summer spectral indices (e.g., tasseled cap brightness and wetness, enhanced vegetation index), which may reflect its seasonal sensitivity to canopy moisture and structure (Beck et al., 2011). Alaskan birch was strongly influenced by post-fire spectral indices (nbr_summer, savi_summer), directly reflecting the empirical link between vegetation greenness and post-fire recovery in this early-successional species (Figure 5) (Schuler, 2004). Trembling aspen also showed strong influence from spatial and topographic variables in the RS-RF model (e.g., latitude, longitude, digital surface model), highlighting its niche edaphic and topographic preferences (Roland et al., 2013). These patterns are partially consistent with known life history strategies: black spruce is strongly tied to cold, lowland environments and surface organic layers (Viereck, 1992); white spruce exhibits mid-successional traits and canopy sensitivity (Chapin, 2006); and both birch and aspen are disturbance-adapted pioneers that rapidly colonize post-fire landscapes (Johnstone et al., 2010a; Roland et al., 2013).

Conversely, the process-based LANDIS-II model emphasized internal ecological mechanisms. Dead and live organic matter pools (DeadRoots, DeadWood, finefuels) consistently ranked as top predictors across all species. This reflects LANDIS-II's mechanistic representation of carbon cycling, where carbon accumulation and decomposition are tied to these pools. Weiss et al. (2023) similarly found that the percentage of aboveground biomass killed by wildfire, a measure of fire severity, was the strongest predictor of post-fire vegetation trajectories, supporting the importance of fuel and carbon pools in shaping successional outcomes. Indirect drivers like uphill aspect and wind direction indicate LANDIS-II's sensitivity to fire regime factors influencing succession, complementing Weiss et al.'s emphasis on fire severity gradients.

It is important to note that the different drivers identified by each model do not necessarily contradict each other. Rather, they reflect different underlying frameworks: RS-RF identifies statistical predictors of observed outcomes, while LANDIS-II represents mechanistic drivers of

ecosystem processes. Together, these complementary insights from RS-RF and LANDIS-II deepen our understanding of aboveground carbon dynamics by linking spatial patterns and empirical observations with the underlying ecological processes driving post-fire forest succession.

4.4 Model Calibration Challenges

The observed discrepancies in carbon estimates, species dominance, and identified drivers highlight the inherent challenges of accurately representing complex ecological processes in remote, rapidly changing landscapes. A key factor is the contrasting calibration approaches and data sources. RS-RF models, empirically driven by remote sensing imagery and ground observations, are robust for interpolation and capturing observed patterns. However, these models are most effective for estimating biomass within the domain of existing observational data and are not well suited for extrapolating beyond baseline conditions (Goetz et al., 2009). This restricts their capacity to anticipate emerging community types under novel climate or disturbance regimes. Moreover, existing data is often spatially limited and might not capture the full range of variability across large landscapes.

Process-based models like LANDIS-II, conversely, demand extensive parameterization of ecological processes (growth, regeneration, competition, disturbance). Accurate calibration is crucial and highly sensitive to available empirical data (Reese et al., 2025). For Interior Alaska, species-specific growth and regeneration parameters are often derived from sparse plot data or generalized regional studies, potentially leading to the overestimation of biomass accumulation observed in LANDIS-II (Ameray et al., 2024). Moreover, LANDIS-II's mechanistic fire simulations, while driven by fuel dynamics and climate (e.g., Fire Weather Index), are highly sensitive to the calibration of ignition probabilities and spread (Weiss et al., 2023). This demonstrates inherent difficulty in precisely capturing complex, real-world ecological dynamics within a generalized framework.

4.5 Study Limitations

Despite the valuable insights, this study has several limitations. First, the accuracy of both modeling approaches is inherently constrained by the quality and spatial representativeness of the

underlying input data. The field observations used for RS-RF training and validation, while highly useful, may not fully capture the full range of variability across the vast and heterogeneous Interior Alaskan landscape. Similarly, LANDIS-II's parameterization relies on available ecological data, which can be sparse for specific species or processes in remote boreal environments. Another limitation is access to "unfuzzed" and high-resolution forest inventory data in remote regions (e.g., contrasting data from customized regional efforts like CAFI vs. standard FIA plots), which makes comprehensive calibration for detailed process models particularly demanding. In this study, LANDIS-II benefitted from access to unfuzzed data from FIA, while RS-RF relied solely on CAFI field observations. This distinction reflects broader challenges in securing data-sharing agreements and accessing high-quality inventory data under current resource constraints. Maintaining and expanding access to detailed field data remains critical for improving ecological forecasting across modeling frameworks. Third, while this study compared temporal trends and spatial dominance, a more direct fine-scale spatial validation of LANDIS-II outputs against empirical data would further clarify localized model performance. Moreover, the two models operate at different spatial and temporal resolutions (e.g., RS-RF: annually at 30 m, LANDIS-II: daily and annually at 200 m) which complicates pixel-to-pixel comparisons. Lastly, the focus on aboveground carbon, while important, does not encompass the entire ecosystem carbon budget; considering belowground carbon dynamics and their interactions with fire and vegetation shifts remain a crucial avenue for future investigation.

5. CONCLUSION

This study highlights the complementary strengths of data-driven (RS-RF) and process-based (LANDIS-II) modeling approaches in assessing aboveground carbon dynamics in interior Alaska. The RS-RF model demonstrated closer empirical fit to CAFI observed data and effectively captured immediate, fine-scale disturbance-related changes in carbon stocks, particularly for early-successional hardwoods. LANDIS-II provided a mechanistic framework for simulating long-term ecological processes and their influence on carbon cycling, with its initial conditions derived from FIA data. Although LANDIS-II showed lower agreement with observed data, it exhibited greater temporal variability and has the capacity to offer a mechanistic understanding that is crucial for simulating long-term carbon dynamics under changing environmental conditions and altered disturbance regimes.

Integrating these complementary approaches holds significant promise for advancing forest carbon assessments. Remote sensing-derived carbon maps could initialize and constrain process-based simulations, offering a more accurate representation of current conditions. Conversely, the mechanistic understanding from process-based models could inform the interpretation of remote sensing trends, helping to identify underlying drivers of change not directly captured by spectral indices. Future research should prioritize developing robust data assimilation techniques to effectively fuse these modeling frameworks. Such integration will yield more reliable and comprehensive carbon assessments, enhancing our ability to understand and project the future of boreal forest ecosystems in a rapidly changing climate.

6. REFERENCES

Abramoff, R. Z., Davidson, E. A., & Finzi, A. C. (2017). A parsimonious modular approach to building a mechanistic belowground carbon and nitrogen model. *Journal of Geophysical Research: Biogeosciences*, *122*(9), 2418–2434. https://doi.org/10.1002/2017JG003796

Alaska Center for Conservation Science (2017) Alaska vegetation and wetland composite map. https://accscatalog.uaa. alaska.edu/dataset/alaska-vegetation-and-wetland-compo site. Accessed 17 Jan 2022

Alexander, H. D., Mack, M. C., Goetz, S., Beck, P. S. A., & Belshe, E. F. (2012). Implications of increased deciduous cover on stand structure and aboveground carbon pools of Alaskan boreal forests. *Ecosphere*, *3*(5), art45. https://doi.org/10.1890/ES11-00364.1

Ameray, A., Cavard, X., Cyr, D., Valeria, O., Girona, M. M., & Bergeron, Y. (2024). One century of carbon dynamics in the eastern Canadian boreal forest under various management strategies and climate change projections. *Ecological Modelling*, *498*, 110894. https://doi.org/10.1016/j.ecolmodel.2024.110894

Apps, M. J., Kurz, W. A., Luxmoore, R. J., Nilsson, L. O., Sedjo, R. A., Schmidt, R., Simpson, L. G., & Vinson, T. S. (1993). Boreal forests and tundra. *Water, Air, and Soil Pollution*, *70*(1), 39–53. https://doi.org/10.1007/BF01104987

Armatas, C. A., Campbell, R. M., Watson, A. E., Borrie, W. T., Christensen, N., & Venn, T. J. (2018). An integrated approach to valuation and tradeoff analysis of ecosystem services for national forest decision-making. *Ecosystem Services*, *33*, 1–18. https://doi.org/10.1016/j.ecoser.2018.07.007

Beck, P. S. A., Juday, G. P., Alix, C., Barber, V. A., Winslow, S. E., Sousa, E. E., Heiser, P., Herriges, J. D., & Goetz, S. J. (2011). Changes in forest productivity across Alaska consistent with biome shift. *Ecology Letters*, *14*(4), 373–379. https://doi.org/10.1111/j.1461-0248.2011.01598.x

Benesty, J., Chen, J., Huang, Y., & Cohen, I. (2009). Pearson Correlation Coefficient. In I. Cohen, Y. Huang, J. Chen, & J. Benesty (Eds.), *Noise Reduction in Speech Processing* (pp. 1–4). Springer. https://doi.org/10.1007/978-3-642-00296-0_5

Bieniek, P. A., Bhatt, U. S., Walsh, J. E., Rupp, T. S., Zhang, J., Krieger, J. R., & Lader, R. (2016). *Dynamical Downscaling of ERA-Interim Temperature and Precipitation for Alaska*. https://doi.org/10.1175/JAMC-D-15-0153.1

Boston, T., Van Dijk, A., Larraondo, P. R., & Thackway, R. (2022). Comparing CNNs and Random Forests for Landsat Image Segmentation Trained on a Large Proxy Land Cover Dataset. *Remote Sensing*, *14*(14), Article 14. https://doi.org/10.3390/rs14143396

Breiman, L., Cutler, A., Liaw, A., & Wiener, M. (2002). *randomForest: Breiman and Cutlers Random Forests for Classification and Regression* (p. 4.7-1.2) [Dataset]. https://doi.org/10.32614/CRAN.package.randomForest

Cahoon, S. M. P., Baer, K. C., Legner, K., Winton, L., Dubois, G., Putman, W., Sullivan, P., Marcille, K. C., Andersen, H., Strunk, J., Smith, R. J., Chase, J., Christensen, G., Terzibashian, J., & Gray, A. (2022). Forest resources of the Tanana unit, Alaska: 2018.

Gen. Tech. Rep. PNW-GTR-1005. Portland, OR: U.S. Department of Agriculture, Forest Service, Pacific Northwest Research Station. 92 p., *1005*. https://doi.org/10.2737/PNW-GTR-1005

Chapin, F. S. (2006). *Alaska's Changing Boreal Forest*. Oxford University Press, USA.

Chapin, F. S., Trainor, S. F., Huntington, O., Lovecraft, A. L., Zavaleta, E., Natcher, D. C., McGuire, A. D., Nelson, J. L., Ray, L., Calef, M., Fresco, N., Huntington, H., Rupp, T. S., DeWilde, L., & Naylor, R. L. (2008). Increasing Wildfire in Alaska's Boreal Forest: Pathways to Potential Solutions of a Wicked Problem. *BioScience*, *58*(6), 531–540. https://doi.org/10.1641/B580609

Chen, X., Yang, K., Ma, J., Jiang, K., Gu, X., & Peng, L. (2024). Aboveground Biomass Inversion Based on Object-Oriented Classification and Pearson–mRMR–Machine Learning Model. *Remote Sensing*, *16*(9), Article 9. https://doi.org/10.3390/rs16091537

Cutler, D. R., Edwards, T. C., Beard, K. H., Cutler, A., Hess, K. T., Gibson, J., & Lawler, J. J. (2007). Random forests for classification in ecology. *Ecology*, *88*(11), 2783–2792. https://doi.org/10.1890/07-0539.1

Dale, V. H., Joyce, L. A., McNulty, S., Neilson, R. P., Ayres, M. P., Flannigan, M. D., Hanson, P. J., Irland, L. C., Lugo, A. E., Peterson, C. J., Simberloff, D., Swanson, F. J., Stocks, B. J., & Wotton, B. M. (2001). Climate Change and Forest Disturbances: Climate change can affect forests by altering the frequency, intensity, duration, and timing of fire, drought, introduced species, insect and pathogen outbreaks, hurricanes, windstorms, ice storms, or landslides. *BioScience*, *51*(9), 723–734. https://doi.org/10.1641/0006-3568(2001)051[0723:CCAFD]2.0.CO;2

Dubayah, R. O., & Drake, J. B. (2000). Lidar Remote Sensing for Forestry. *Journal of Forestry*, *98*(6), 44–46. https://doi.org/10.1093/jof/98.6.44

Extension-Output-Biomass-Community/docs/LANDIS-II Biomass Community Output v3.0 User Guide.pdf at master · LANDIS-II-Foundation/Extension-Output-Biomass-Community. (n.d.). GitHub. Retrieved May 27, 2025, from https://github.com/LANDIS-II-Foundation/Extension-Output-Biomass-Community/blob/master/docs/LANDIS-II%20Biomass%20Community%20Output%20v3.0%20User%20Guide.pdf

Fisher, J. B., Sikka, M., Oechel, W. C., Huntzinger, D. N., Melton, J. R., Koven, C. D., Ahlström, A., Arain, M. A., Baker, I., Chen, J. M., Ciais, P., Davidson, C., Dietze, M., El-Masri, B., Hayes, D., Huntingford, C., Jain, A. K., Levy, P. E., Lomas, M. R., … Miller, C. E. (2014). Carbon cycle uncertainty in the Alaskan Arctic. *Biogeosciences*, *11*(15), 4271–4288. https://doi.org/10.5194/bg-11-4271-2014

Fleming, R. A. (2001). The Weibull model and an ecological application: Describing the dynamics of foliage biomass on Scots pine. *Ecological Modelling*, *138*(1), 309–319. https://doi.org/10.1016/S0304-3800(00)00410-5

Flerchinger, G. N., & Cooley, K. R. (2000). A ten-year water balance of a mountainous semi-arid watershed. *Journal of Hydrology*, *237*(1), 86–99. https://doi.org/10.1016/S0022-1694(00)00299-7

Flerchinger, G. N., Cooley ,K. R., & and Deng, Y. (1994). Impacts of spatially and temporally varying snowmelt on subsurface flow in a mountainous watershed: 1. Snowmelt simulation. *Hydrological Sciences Journal*, *39*(5), 507–520. https://doi.org/10.1080/02626669409492771

Flerchinger, G. N., Reba, M. L., Link, T. E., & Marks, D. (2015). Modeling temperature and humidity profiles within forest canopies. *Agricultural and Forest Meteorology*, *213*, 251–262. https://doi.org/10.1016/j.agrformet.2015.07.007

GeoMAC (2019) Historic perimeters combined 2000–2018. U.S. geological survey. Accessed 14 Aug 2020

GeoMAC (2020) Historic Perimeters 2019, U.S. geological survey. https://data-nifc.opendata.arcgis.com/datasets/ nifc::historic-perimeters-2019/about. Accessed 14 Aug 2020

Goetz, S. J., Baccini, A., Laporte, N. T., Johns, T., Walker, W., Kellndorfer, J., Houghton, R. A., & Sun, M. (2009). Mapping and monitoring carbon stocks with satellite observations: A comparison of methods. *Carbon Balance and Management*, *4*(1), 2. https://doi.org/10.1186/1750-0680-4-2

Gorelick, N., Hancher, M., Dixon, M., Ilyushchenko, S., Thau, D., & Moore, R. (2017). Google Earth Engine: Planetary-scale geospatial analysis for everyone. *Remote Sensing of Environment*, *202*, 18–27. https://doi.org/10.1016/j.rse.2017.06.031

Gustafson, E. J. (2013). When relationships estimated in the past cannot be used to predict the future: Using mechanistic models to predict landscape ecological dynamics in a changing world. *Landscape Ecology*, *28*(8), 1429–1437. https://doi.org/10.1007/s10980-013-9927-4

Gustafson, E. J., Lucash, M. S., Shvidenko, A. Z., Sturtevant, B. R., Miranda, B. R., Schepaschenko, D., & Matsumoto, H. (2024). Climate change and disturbance interact to alter landscape reflectivity (albedo) in boreal forests across a large latitudinal gradient in Siberia. *Science of The Total Environment*, *956*, 177043. https://doi.org/10.1016/j.scitotenv.2024.177043

Hinzman, L. D., & Viereck, L. A. (2006). Climate and Permafrost Dynamics of the Alaskan Boreal Forest. In F. S. Chapin, M. W. Oswood, K. Van Cleve, L. A. Viereck, & D. L. Verbyla (Eds.), *Alaska's Changing Boreal Forest* (p. 0). Oxford University Press. https://doi.org/10.1093/oso/9780195154313.003.0008

Hurni, K., Van Den Hoek, J., & Fox, J. (2019). Assessing the spatial, spectral, and temporal consistency of topographically corrected Landsat time series composites across the mountainous forests of Nepal. *Remote Sensing of Environment*, *231*, 111225. https://doi.org/10.1016/j.rse.2019.111225

Jafarov, E. E., Marchenko, S. S., & Romanovsky, V. E. (2012). Numerical modeling of permafrost dynamics in Alaska using a high spatial resolution dataset. *The Cryosphere*, *6*(3), 613–624. https://doi.org/10.5194/tc-6-613-2012

Jarvis, P. G. (1997). The interpretation of the variations in leaf water potential and stomatal conductance found in canopies in the field. *Philosophical Transactions of the Royal Society of London. B, Biological Sciences*, *273*(927), 593–610. https://doi.org/10.1098/rstb.1976.0035

Jenkins, J. C., Chojnacky, D. C., Heath, L. S., & Birdsey, R. A. (2004). *Comprehensive database of diameter-based biomass regressions for North American tree species* (No. NE-GTR-319; p. NE-GTR-319). U.S. Department of Agriculture, Forest Service, Northeastern Research Station. https://doi.org/10.2737/NE-GTR-319

Johnstone, J. F., Chapin, F. S., Hollingsworth, T. N., Mack, M. C., Romanovsky, V., & Turetsky, M. (2010). Fire, climate change, and forest resilience in interior AlaskaThis article is one of a selection of papers from The Dynamics of Change in Alaska's Boreal Forests: Resilience and Vulnerability in Response to Climate Warming. *Canadian Journal of Forest Research*, *40*(7), 1302–1312. https://doi.org/10.1139/X10-061

Johnstone, J. F., Hollingsworth, T. N., Chapin Iii, F. S., & Mack, M. C. (2010). Changes in fire regime break the legacy lock on successional trajectories in Alaskan boreal forest. *Global Change Biology*, *16*(4), 1281–1295. https://doi.org/10.1111/j.1365-2486.2009.02051.x

Johnstone, J. F., & Kasischke, E. S. (2005). Stand-level effects of soil burn severity on postfire regeneration in a recently burned black spruce forest. *Canadian Journal of Forest Research*, *35*(9), 2151–2163. https://doi.org/10.1139/x05-087

Kasischke, E. S., Verbyla, D. L., Rupp, T. S., McGuire, A. D., Murphy, K. A., Jandt, R., Barnes, J. L., Hoy, E. E., Duffy, P. A., Calef, M., & Turetsky, M. R. (2010). Alaska's changing fire regime — implications for the vulnerability of its boreal forestsThis article is one of a selection of papers from The Dynamics of Change in Alaska's Boreal Forests: Resilience and Vulnerability in Response to Climate Warming. *Canadian Journal of Forest Research*, *40*(7), 1313–1324. https://doi.org/10.1139/X10-098

Kasischke, E. S., Verbyla, D. L., Rupp, T. S., McGuire, A. D., Murphy, K. A., Jandt, R., Barnes, J. L., Hoy, E. E., Duffy, P. A., Calef, M., & Turetsky, M. R. (2022). Alaska's changing fire regime—Implications for the vulnerability of its boreal forests. *Canadian Journal of Forest Research. 40: 1313-1324*. https://research.fs.usda.gov/treesearch/38929

Kuhn, M., & Silge, J. (2022). *Tidy Modeling with R: A Framework for Modeling in the Tidyverse*. O'Reilly Media, Inc.

Lader, R., Walsh, J. E., Bhatt, U. S., & Bieniek, P. A. (2017). *Projections of Twenty-First-Century Climate Extremes for Alaska via Dynamical Downscaling and Quantile Mapping*. https://doi.org/10.1175/JAMC-D-16-0415.1

Lamping, J., Lucash, M., Bell, D. M., Irvine, D. R., & Gregory, M. (2025). Moderate-resolution mapping of aboveground biomass stocks, forest structure, and composition in coastal Alaska and British Columbia. *Forest Ecology and Management*, *583*, 122576. https://doi.org/10.1016/j.foreco.2025.122576

Lefsky, M. A., Cohen, W. B., Harding, D. J., Parkers, G. G., Acker, S. A., & Gower, S. T. (2002). Lidar remote sensing of above-ground biomass in three biomes. *Global Ecology & Biogeography. 11: 393-399*. https://research.fs.usda.gov/treesearch/24647

Li, Y., Li, M., Li, C., & Liu, Z. (2020). Forest aboveground biomass estimation using Landsat 8 and Sentinel-1A data with machine learning algorithms. *Scientific Reports*, *10*(1), 9952. https://doi.org/10.1038/s41598-020-67024-3

Lucash, M. S., Marshall, A. M., Weiss, S. A., McNabb, J. W., Nicolsky, D. J., Flerchinger, G. N., Link, T. E., Vogel, J. G., Scheller, R. M., Abramoff, R. Z., & Romanovsky, V. E. (2023). Burning trees in frozen soil: Simulating fire, vegetation, soil, and hydrology in the boreal forests of Alaska. *Ecological Modelling*, *481*, 110367. https://doi.org/10.1016/j.ecolmodel.2023.110367

Marchenko, S., Romanovsky, V., Tipenko, G., 2008. Numerical modeling of spatial permafrost dynamics in Alaska. In: Proceedings of the Ninth International Conference on Permafrost. Institute of Northern Engineering, University of Alaska Fairbanks, pp. 1125–1130.

Marshall, A. M., Link, T. E., Flerchinger, G. N., & Lucash, M. S. (2021). Importance of Parameter and Climate Data Uncertainty for Future Changes in Boreal Hydrology. *Water Resources Research*, *57*(8), e2021WR029911. https://doi.org/10.1029/2021WR029911

Massey, R., Rogers, B. M., Berner, L. T., Cooperdock, S., Mack, M. C., Walker, X. J., & Goetz, S. J. (2023). Forest composition change and biophysical climate feedbacks across boreal North America. *Nature Climate Change*, *13*(12), 1368–1375. https://doi.org/10.1038/s41558-023-01851-w

Masson-Delmotte, V., Zhai, P., Pirani, A., Connors, S. L., Péan, C., Berger, S., Caud, N., Chen, Y., Goldfarb, L., Gomis, M. I., Huang, M., Leitzell, K., Lonnoy, E., Matthews, J. B. R., Maycock, T. K., Waterfield, T., Yelekçi, Ö., Yu, R., & Zhou, B. (Eds.). (2021). *Climate Change 2021: The Physical Science Basis. Contribution of Working Group I to the Sixth Assessment Report of the Intergovernmental Panel on Climate Change*. Cambridge University Press. https://doi.org/10.1017/9781009157896

Mekonnen, Z. A., Riley, W. J., Randerson, J. T., Grant, R. F., & Rogers, B. M. (2019). Expansion of high-latitude deciduous forests driven by interactions between climate warming and fire. *Nature Plants*, *5*(9), 952–958. https://doi.org/10.1038/s41477-019-0495-8

Menne MJ, Durre I, Vose RS et al (2012) An overview of the global historical climatology network-daily database. J Atmos Ocean Technol 29:897–910.

Mladenoff, D. J. (2004). LANDIS and forest landscape models. *Ecological Modelling*, *180*(1), 7–19. https://doi.org/10.1016/j.ecolmodel.2004.03.016

Nenzén, H. K., Price, D. T., Boulanger, Y., Taylor, A. R., Cyr, D., & Campbell, E. (2020). Projected climate change effects on Alberta's boreal forests imply future challenges for oil sands reclamation. *Restoration Ecology*, *28*(1), 39–50. https://doi.org/10.1111/rec.13051

Nicolsky, D. J., Romanovsky, V. E., & Panteleev, G. G. (2009). Estimation of soil thermal properties using in-situ temperature measurements in the active layer and permafrost. *Cold Regions Science and Technology*, *55*(1), 120–129. https://doi.org/10.1016/j.coldregions.2008.03.003

Orndahl, K. M., Berner, L. T., Macander, M. J., Arndal, M. F., Alexander, H. D., Humphreys, E. R., Loranty, M. M., Ludwig, S. M., Nyman, J., Juutinen, S., Aurela, M., Mikola, J., Mack, M. C., Rose, M., Vankoughnett, M. R., Iversen, C. M., Kumar, J., Salmon, V. G., Yang, D., … Goetz, S. J. (2025). Next generation Arctic vegetation maps: Aboveground plant biomass and woody dominance mapped at 30 m resolution across the tundra biome. *Remote Sensing of Environment*, *323*, 114717. https://doi.org/10.1016/j.rse.2025.114717

Osterkamp, T. E., & Romanovsky, V. E. (1999). Evidence for warming and thawing of discontinuous permafrost in Alaska. *Permafrost and Periglacial Processes*, *10*(1), 17–37. https://doi.org/10.1002/(SICI)1099-1530(199901/03)10:1<17::AID-PPP303>3.0.CO;2-4

Pan, Y., Birdsey, R. A., Fang, J., Houghton, R., Kauppi, P. E., Kurz, W. A., Phillips, O. L., Shvidenko, A., Lewis, S. L., Canadell, J. G., Ciais, P., Jackson, R. B., Pacala, S. W., McGuire, A. D., Piao, S., Rautiainen, A., Sitch, S., & Hayes, D. (2011). A Large and Persistent Carbon Sink in the World's Forests. *Science*, *333*(6045), 988–993. https://doi.org/10.1126/science.1201609

Parton, W. J., Ojima, D. S., Cole, C. V., & Schimel, D. S. (1994). A General Model for Soil Organic Matter Dynamics: Sensitivity to Litter Chemistry, Texture and Management. In *Quantitative Modeling of Soil Forming Processes* (pp. 147–167). John Wiley & Sons, Ltd. https://doi.org/10.2136/sssaspecpub39.c9

Payette, S. (1992). Fire as a controlling process in the North American boreal forest. In G. B. Bonan, H. H. Shugart, & R. Leemans (Eds.), *A Systems Analysis of the Global Boreal Forest* (pp. 144–169). Cambridge University Press. https://doi.org/10.1017/CBO9780511565489.006

Reese, G. C., Sturtevant, B. R., Dymond, C. C., Quigley, K. M., Duveneck, M. J., Lucash, M. S., Gustafson, E. J., Scheller, R. M., Russell, M. B., & Miranda, B. R. (2025). Best practices for calibration of forest landscape models using fine-scaled reference information. *Canadian Journal of Forest Research*, *55*, 1–19. https://doi.org/10.1139/cjfr-2024-0085

Richardson, F. L. (1922) Weather prediction by numerical process. Cambridge (University Press), 1922. 4°. Pp. Xii + 236. 30s.net. (1922). *Quarterly Journal of the Royal Meteorological Society*, *48*(203), 282–284. https://doi.org/10.1002/qj.49704820311

Roland, C. A., Schmidt, J. H., & Nicklen, E. F. (2013). Landscape-scale patterns in tree occupancy and abundance in subarctic Alaska. *Ecological Monographs*, *83*(1), 19–48. https://doi.org/10.1890/11-2136.1

Scheller, R., Kretchun, A., Hawbaker, T. J., & Henne, P. D. (2019). A landscape model of variable social-ecological fire regimes. *Ecological Modelling*, *401*, 85–93. https://doi.org/10.1016/j.ecolmodel.2019.03.022

Scheller, R. M., Domingo, J. B., Sturtevant, B. R., Williams, J. S., Rudy, A., Gustafson, E. J., & Mladenoff, D. J. (2007). Design, development, and application of LANDIS-II, a spatial landscape simulation model with flexible temporal and spatial resolution. *Ecological Modelling*, *201*(3), 409–419. https://doi.org/10.1016/j.ecolmodel.2006.10.009

Scheller, R. M., Hua, D., Bolstad, P. V., Birdsey, R. A., & Mladenoff, D. J. (2011). The effects of forest harvest intensity in combination with wind disturbance on carbon dynamics in Lake States Mesic Forests. *Ecological Modelling*, *222*(1), 144–153. https://doi.org/10.1016/j.ecolmodel.2010.09.009

Scheller, R. M., & Mladenoff, D. J. (2004). A forest growth and biomass module for a landscape simulation model, LANDIS: Design, validation, and application. *Ecological Modelling*, *180*(1), 211–229. https://doi.org/10.1016/j.ecolmodel.2004.01.022

Schuler, T. M. (2004). Fifty years of partial harvesting in a mixed mesophytic forest: Composition and productivity. *Canadian Journal of Forest Research*, *34*(5), 985–997. https://doi.org/10.1139/x03-262

Schuur, E. a. G., McGuire, A. D., Schädel, C., Grosse, G., Harden, J. W., Hayes, D. J., Hugelius, G., Koven, C. D., Kuhry, P., Lawrence, D. M., Natali, S. M., Olefeldt, D., Romanovsky, V. E., Schaefer, K., Turetsky, M. R., Treat, C. C., & Vonk, J. E. (2015). Climate change and the permafrost carbon feedback. *Nature*, *520*(7546), 171–179. https://doi.org/10.1038/nature14338

Shenoy, A., Johnstone, J. F., Kasischke, E. S., & Kielland, K. (2011). Persistent effects of fire severity on early successional forests in interior Alaska. *Forest Ecology and Management*, *261*(3), 381–390. https://doi.org/10.1016/j.foreco.2010.10.021

Short, K. C. (2014). A spatial database of wildfires in the United States, 1992-2011. *Earth System Science Data*, *6*(1), 1–27. https://doi.org/10.5194/essd-6-1-2014

Shugart, H. (1984). *A theory of forest dynamics: The ecological implications of forest succession models*. https://www.academia.edu/3764046/A_theory_of_forest_dynamics_The_ecological_implications_of_forest_succession_models

Simons-Legaard, E., Legaard, K., & Weiskittel, A. (2015). Predicting aboveground biomass with LANDIS-II: A global and temporal analysis of parameter sensitivity. *Ecological Modelling*, *313*, 325–332. https://doi.org/10.1016/j.ecolmodel.2015.06.033

Simultaneous Heat and Water Model of a Freezing Snow-Residue-Soil System II. Field Verification. (n.d.). Retrieved April 23, 2025, from https://doi.org/10.13031/2013.31041

Soenen, S. A., Peddle, D. R., & Coburn, C. A. (2005). SCS+C: A modified Sun-canopy-sensor topographic correction in forested terrain. *IEEE Transactions on Geoscience and Remote Sensing*, *43*(9), 2148–2159. IEEE Transactions on Geoscience and Remote Sensing. https://doi.org/10.1109/TGRS.2005.852480

Stewart, J. B. (1988). Modelling surface conductance of pine forest. *Agricultural and Forest Meteorology*, *43*(1), 19–35. https://doi.org/10.1016/0168-1923(88)90003-2

Sturtevant, B. R., Scheller, R. M., Miranda, B. R., Shinneman, D., & Syphard, A. (2009). Simulating dynamic and mixed-severity fire regimes: A process-based fire extension for LANDIS-II. *Ecological Modelling*, *220*(23), 3380–3393. https://doi.org/10.1016/j.ecolmodel.2009.07.030

Tadono, T., Ishida, H., Oda, F., Naito, S., Minakawa, K., & Iwamoto, H. (2014). Precise Global DEM Generation by ALOS PRISM. *ISPRS Annals of the Photogrammetry, Remote Sensing and Spatial Information Sciences*, *II–4*, 71–76. https://doi.org/10.5194/isprsannals-II-4-71-2014

Tian, L., Wu, X., Tao, Y., Li, M., Qian, C., Liao, L., & Fu, W. (2023). Review of Remote Sensing-Based Methods for Forest Aboveground Biomass Estimation: Progress, Challenges, and Prospects. *Forests*, *14*(6), Article 6. https://doi.org/10.3390/f14061086

Torre-Tojal, L., Bastarrika, A., Boyano, A., Lopez-Guede, J. M., & Graña, M. (2022). Above-ground biomass estimation from LiDAR data using random forest algorithms. *Journal of Computational Science*, *58*, 101517. https://doi.org/10.1016/j.jocs.2021.101517

Turetsky, M. R., Kane, E. S., Harden, J. W., Ottmar, R. D., Manies, K. L., Hoy, E., & Kasischke, E. S. (2011). Recent acceleration of biomass burning and carbon losses in Alaskan forests and peatlands. *Nature Geoscience*, *4*(1), 27–31. https://doi.org/10.1038/ngeo1027

USGS (2020a) Alaska 2 Arc-second Digital Elevation Models (DEMs). https://data.usgs.gov/datacatalog/data/USGS: 4bd95204-7a29-4bd4-acce-00551ecaf47a

USGS (2020b) LANDFIRE 2020b fuel characteristic classification system (FCCS) AK 2022 capable fuels. https:// landfire.gov/metadata/lf2020b/AK/LA22_FCCS_220. html.

Van Cleve, K., Chapin, F. S., Ruess, R., & Bonanza Creek LTER. (2023). *Bonanza Creek LTER: Tree Inventory Data from 1989 to present at Core research sites in Interior Alaska* [Dataset]. Environmental Data Initiative. https://doi.org/10.6073/PASTA/DAE1E19CD2B398F7E979155D858B386C

Van Cleve, K., Dyrness, C. T., Viereck, L. A., Fox, J., Chapin, F. S., III, & Oechel, W. (1983). Taiga Ecosystems in Interior Alaska. *BioScience*, *33*(1), 39–44. https://doi.org/10.2307/1309243

Van Cleve, K., & Viereck, L. A. (1981). Forest Succession in Relation to Nutrient Cycling in the Boreal Forest of Alaska. In D. C. West, H. H. Shugart, & D. B. Botkin (Eds.), *Forest Succession: Concepts and Application* (pp. 185–211). Springer. https://doi.org/10.1007/978-1-4612-5950-3_13

Viereck, L. A. (1973). Wildfire in the Taiga of Alaska. *Quaternary Research*, *3*(3), 465–495. https://doi.org/10.1016/0033-5894(73)90009-4

Viereck, L. A. (1992). *The Alaska Vegetation Classification*. U.S. Department of Agriculture, Forest Service, Pacific Northwest Research Station.

Viereck, L. A., Dyrness, C. T., Cleve, K. V., & Foote, M. J. (1983). Vegetation, soils, and forest productivity in selected forest types in interior Alaska. *Canadian Journal of Forest Research*, *13*(5), 703–720. https://doi.org/10.1139/x83-101

Walker, X. J., Okano, K., Berner, L. T., Massey, R., Goetz, S. J., Johnstone, J. F., & Mack, M. C. (2023). Shifts in Ecological Legacies Support Hysteresis of Stand Type Conversions in Boreal Forests. *Ecosystems*, *26*(8), 1796–1805. https://doi.org/10.1007/s10021-023-00866-w

Weiss, S. A., Marshall, A. M., Hayes, K. R., Nicolsky, D. J., Buma, B., & Lucash, M. S. (2023). Future transitions from a conifer to a deciduous-dominated landscape are accelerated by greater wildfire activity and climate change in interior Alaska. *Landscape Ecology*, *38*(10), 2569–2589. https://doi.org/10.1007/s10980-023-01733-8

Wells, J. V., Dawson, N., Culver, N., Reid, F. A., & Morgan Siegers, S. (2020). The State of Conservation in North America's Boreal Forest: Issues and Opportunities. *Frontiers in Forests and Global Change*, *3*, 90. https://doi.org/10.3389/ffgc.2020.00090

Wulder, M. A., Roy, D. P., Radeloff, V. C., Loveland, T. R., Anderson, M. C., Johnson, D. M., Healey, S., Zhu, Z., Scambos, T. A., Pahlevan, N., Hansen, M., Gorelick, N., Crawford, C. J., Masek, J. G., Hermosilla, T., White, J. C., Belward, A. S., Schaaf, C., Woodcock, C. E., … Cook, B. D. (2022). Fifty years of Landsat science and impacts. *Remote Sensing of Environment*, *280*, 113195. https://doi.org/10.1016/j.rse.2022.113195

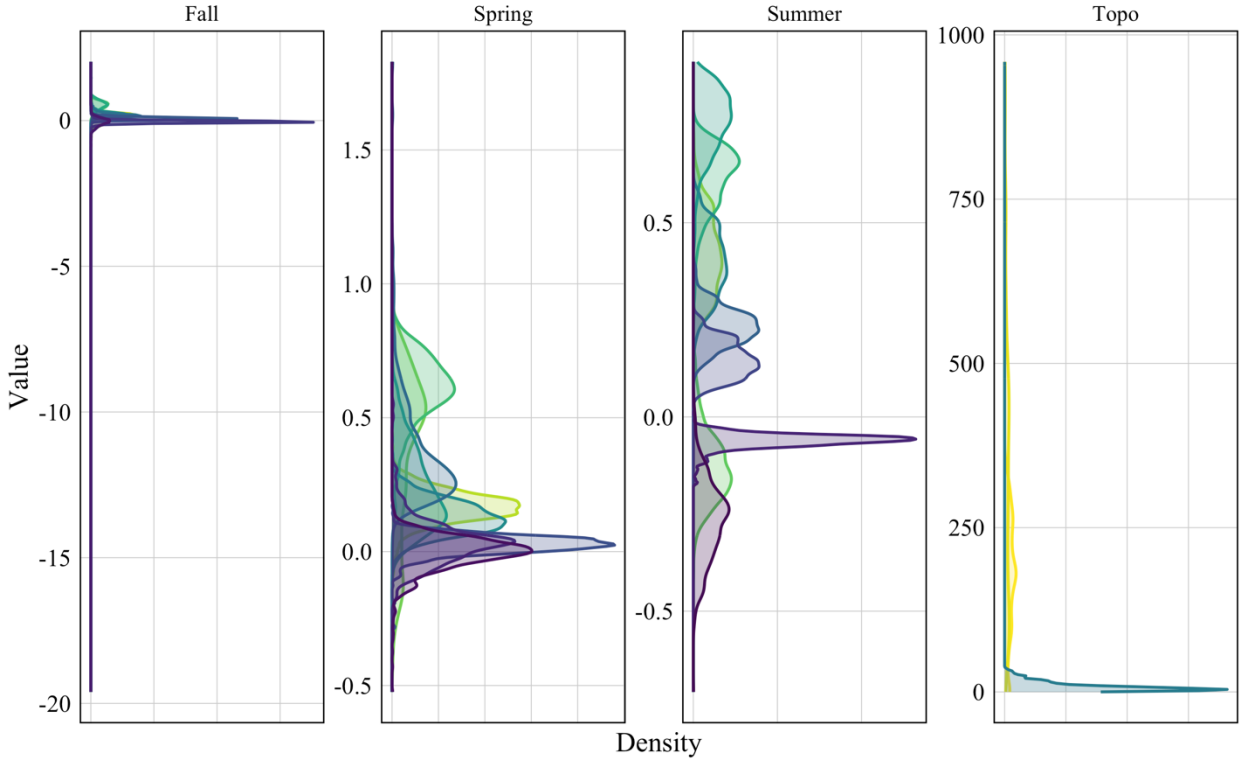

Supplemental Figure 1. *Normalized histograms (density plots) of spectral and topographic features used in Random Forest modeling, grouped by season. Each curve represents a single feature, with spectral variables categorized by Spring, Summer, or Fall based on acquisition season, and topographic features grouped separately. Density values are scaled to enable comparison across variables with differing units and distributions.*

Supplemental Table 1: *Random forest model performance metrics and hyperparameters for predicting aboveground carbon by species. RMSE = Root Mean Square Error; R^2 = coefficient of determination; mtry = number of variables randomly sampled at each split; min n = minimum number of observations in a node; trees = number of decision trees in the forest.*

Species	RMSE	R^2	mtry	min n	trees
Black spruce	57.69	0.75	20	1	600
White spruce	158.64	0.53	20	4	500
Alaskan birch	127.69	0.65	15	1	600
Trembling aspen	169.36	0.42	20	1	500

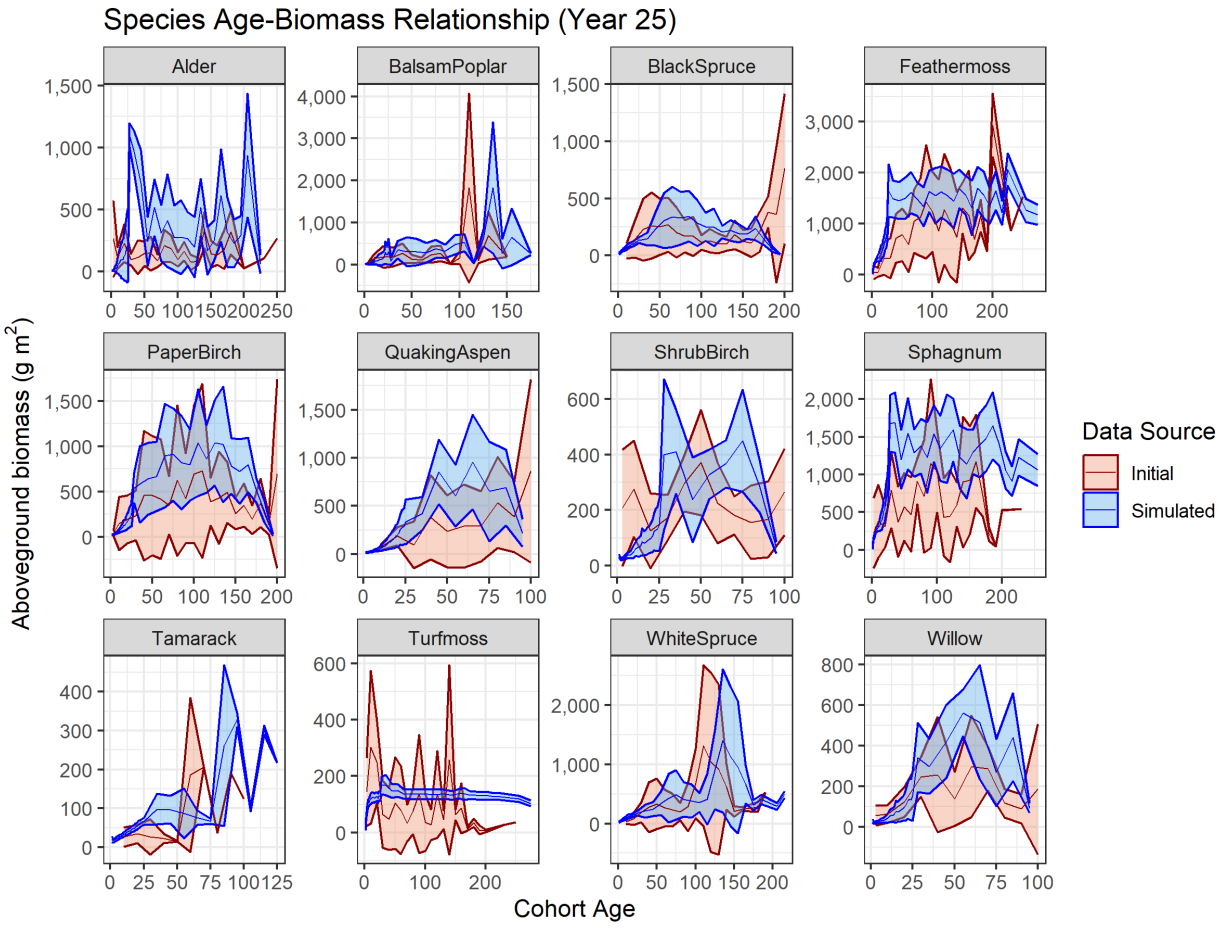

Supplemental Figure 2. *Species age-biomass relationships at Year 25 from LANDIS-II, comparing initial and simulated condition. Each panel displays the aboveground biomass (g m^{-2}) as a function of cohort age for a different species. The 'Initial' data (red lines and shaded area) represents the starting conditions used in the simulation, while the 'Simulated' data (blue lines and shaded area) shows the modeled biomass values after 25 years. The shaded areas represent the variability (e.g., standard deviation or confidence interval) around the mean.*

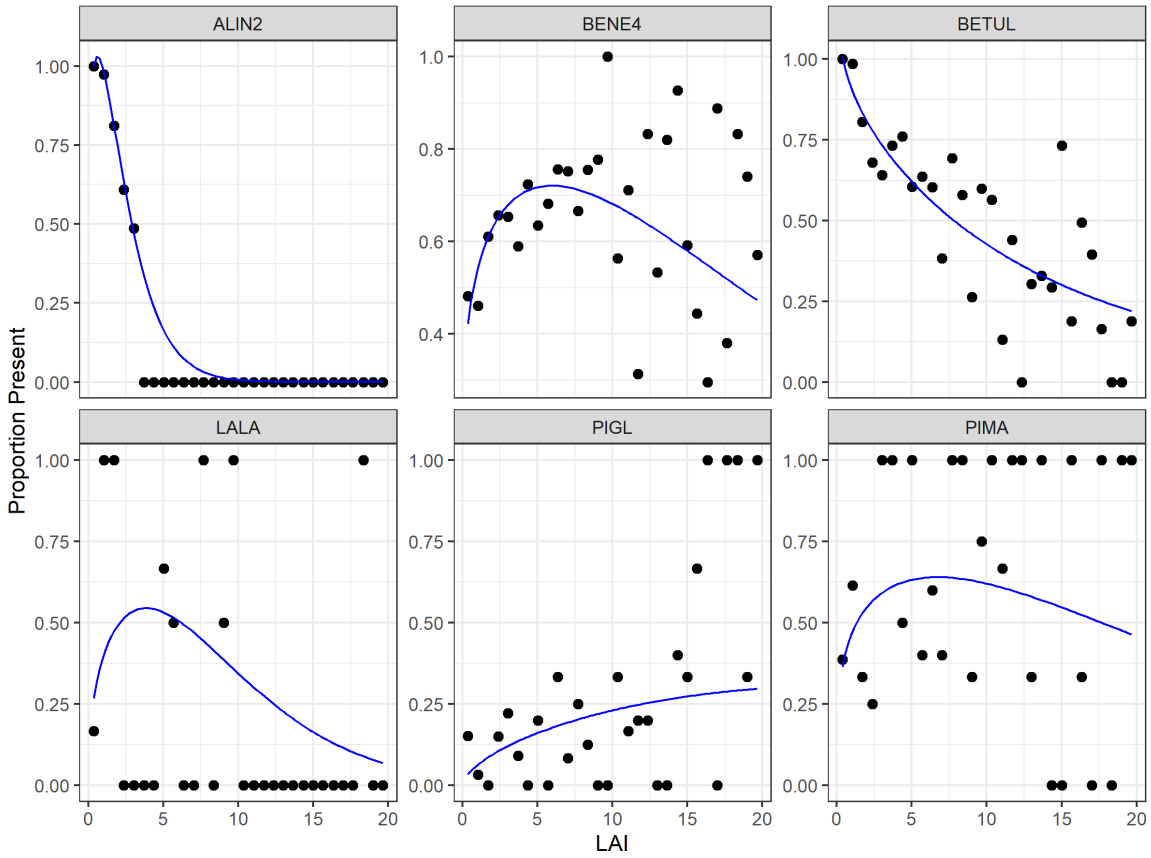

Supplemental Figure 3. *Fitted Weibull distributions for species-specific light establishment parameters. Each panel displays the probability density of seedling establishment as a function of light availability, derived from FIA data. Curves illustrate the unique light response of each species, with corresponding shape and scale parameters.*

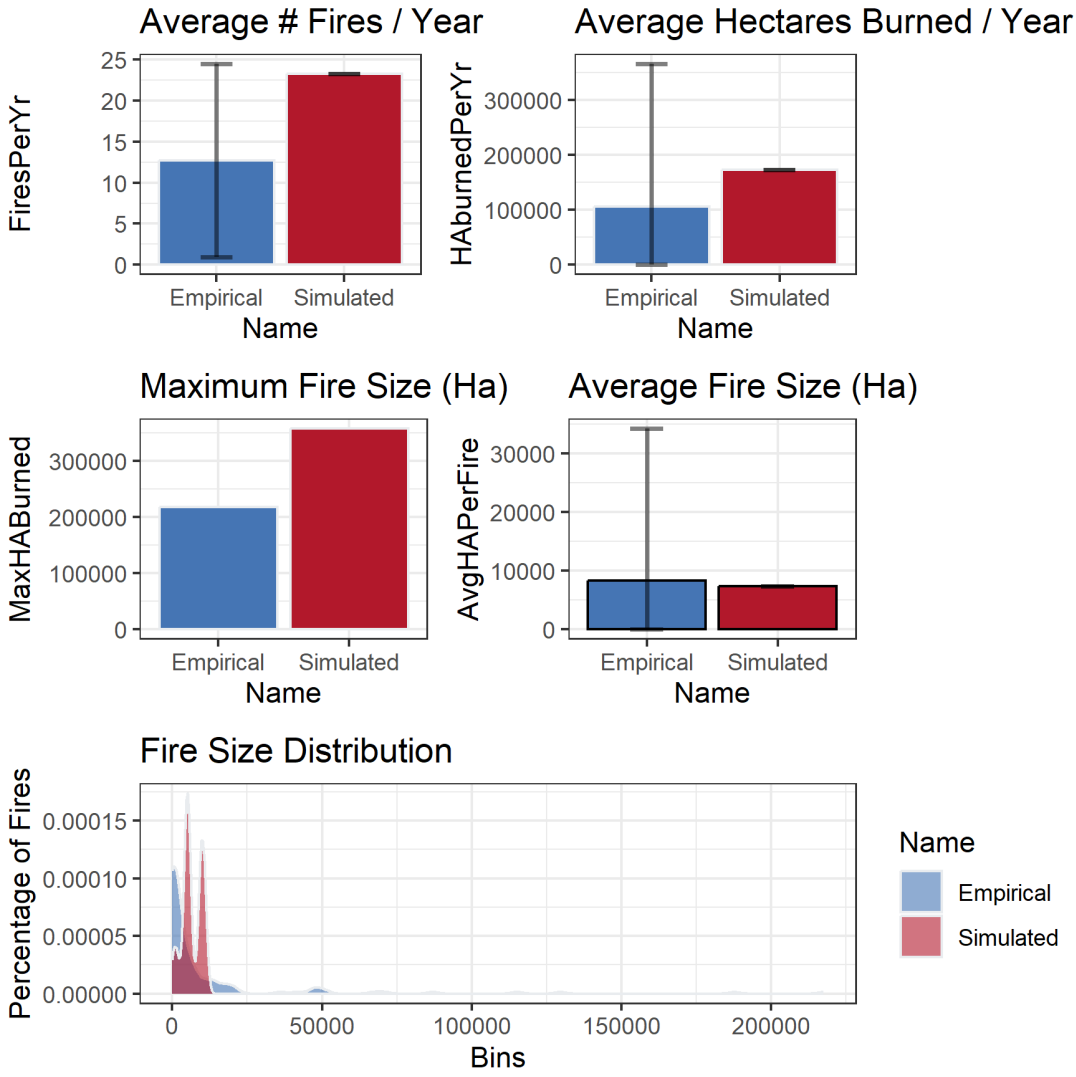

Supplemental Figure 4. *Calibration and validation of the LANDIS-II fire module parameters against empirical fire characteristics. The panels compare simulated fire activity (red bars/distribution) to observed historical records (blue bars/distribution) for key fire metrics in the study area. This includes average number of fires per year, average hectares burned per year, maximum fire size, average fire size, and the overall fire size distribution.*

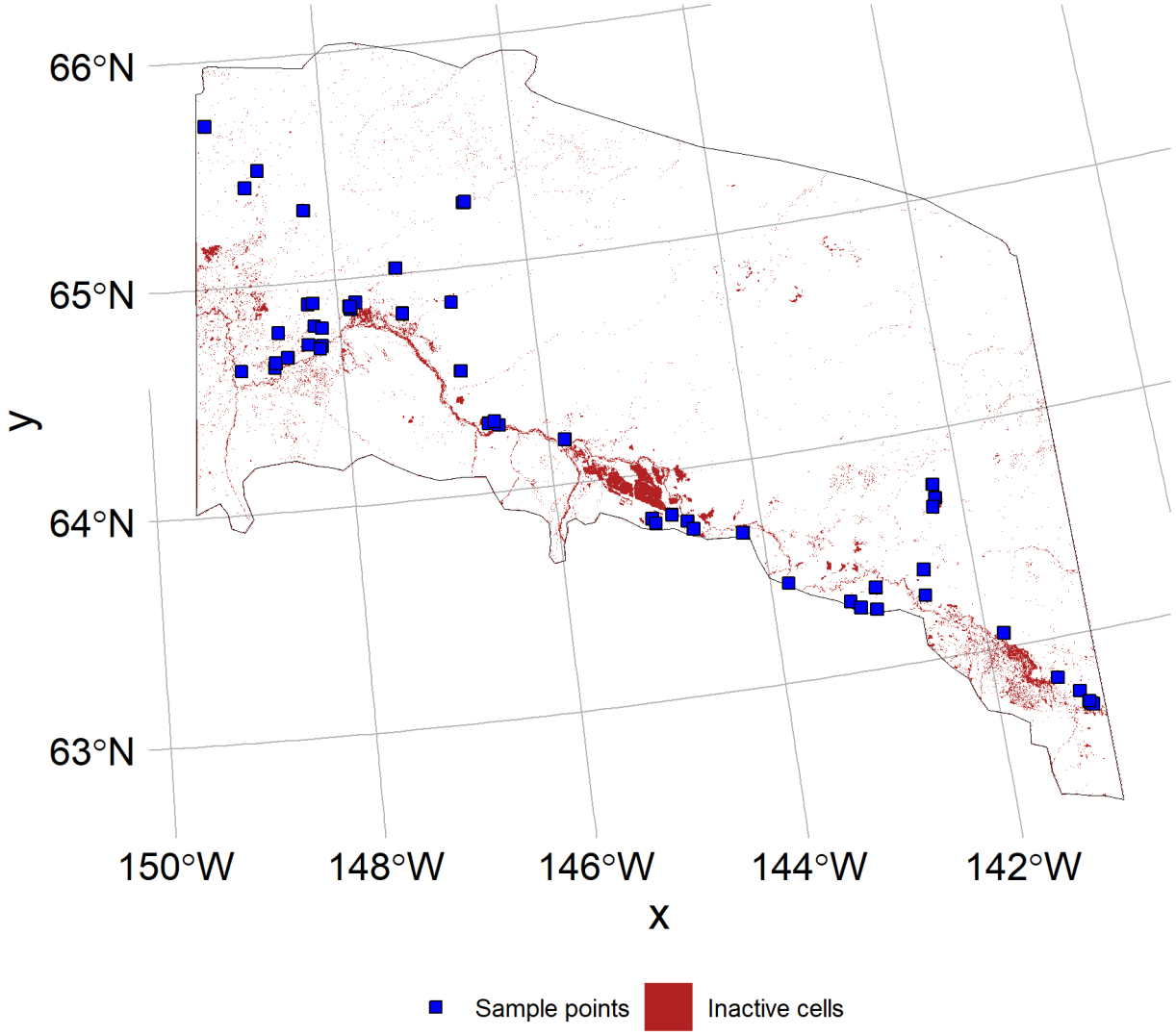

Supplemental Figure 5. *Spatial sampling design for obtaining aboveground C estimates in interior Alaska. The map shows the modeling domain (black outline), with resampled permanent sample locations shown as blue points. Red polygons denote "inactive cells" excluded from the analysis due to persistent water, developed land, or other non-forested cover types.*